



Land surface controls on afternoon precipitation

B. P. Guillod et al.

This discussion paper is/has been under review for the journal Atmospheric Chemistry and Physics (ACP). Please refer to the corresponding final paper in ACP if available.

Land surface controls on afternoon precipitation diagnosed from observational data: uncertainties, confounding factors and the possible role of vegetation interception

B. P. Guillod¹, B. Orlowsky¹, D. Miralles², A. J. Teuling³, P. Blanken⁴, N. Buchmann⁵, P. Ciais⁶, M. Ek⁷, K. L. Findell⁸, P. Gentine⁹, B. R. Lintner¹⁰, R. L. Scott¹¹, B. Van den Hurk¹², and S. I. Seneviratne¹

¹ETH Zurich, Institute for Atmospheric and Climate Science, Zurich, Switzerland

²University of Bristol, School of Geographical Sciences, Bristol, UK

³Wageningen University, Hydrology and Quantitative Water Management Group, Wageningen, the Netherlands

⁴University of Colorado, Department of Geography, Boulder, CO, USA

⁵ETH Zurich, Institute of Agricultural Sciences, Zurich, Switzerland

⁶Laboratoire des Sciences du Climat et de l'Environnement, LSCE, Gif-sur-Yvette, France

⁷National Centers for Environmental Prediction, Suitland, MD, USA

Title Page

Abstract

Introduction

Conclusions

References

Tables

Figures



Back

Close

Full Screen / Esc

Printer-friendly Version

Interactive Discussion



⁸Geophysical Fluid Dynamics Laboratory, Princeton, NJ, USA

⁹Columbia University, Department of Earth and Environmental Engineering, New York, NY, USA

¹⁰Rutgers, The State University of New Jersey, Department of Environmental Sciences, New Brunswick, NJ, USA

¹¹Southwest Watershed Research Center, USDA-ARS, Tucson, AZ, USA

¹²Royal Netherlands Meteorological Institute, KNMI, De Bilt, the Netherlands

Received: 24 September 2013 – Accepted: 24 October 2013 – Published: 7 November 2013

Correspondence to: B. P. Guillod (benoit.guillod@env.ethz.ch) and
S. I. Seneviratne (sonia.seneviratne@env.ethz.ch)

Published by Copernicus Publications on behalf of the European Geosciences Union.

**Land surface
controls on afternoon
precipitation**

B. P. Guillod et al.

Title Page

Abstract

Introduction

Conclusions

References

Tables

Figures



Back

Close

Full Screen / Esc

Printer-friendly Version

Interactive Discussion



Abstract

The feedback between soil moisture and precipitation has long been a topic of interest due to its potential for improving weather and seasonal forecasts. The generally proposed mechanism assumes a control of soil moisture on precipitation via the partitioning of the surface turbulent heat fluxes, as assessed via the Evaporative Fraction, EF, i.e. the ratio of latent heat to the sum of latent and sensible heat, in particular under convective conditions. Our study investigates the poorly understood link between EF and precipitation by investigating the impact of before-noon EF on the frequency of afternoon precipitation over the contiguous US, using a statistical analysis of the relationship between multiple datasets of EF and precipitation. We analyze remote sensing data products (EF from GLEAM, Global Land Evaporation: the Amsterdam Methodology, based on satellite observations; and radar precipitation from NEXRAD, the NEXt generation weather RADar system), FLUXNET station data, and the North American Regional Reanalysis (NARR). While most datasets agree on the existence of regions of positive relationship between between EF and precipitation in the Eastern and Southwestern US, observation-based estimates (GLEAM, NEXRAD and to some extent FLUXNET) also indicate a strong relationship in the Central US which is not found in NARR. Investigating these differences, we find that much of these relationships can be explained by precipitation persistence alone, with ambiguous results on the additional role of EF in causing afternoon precipitation. Regional analyses reveal contrasting mechanisms over different regions. Over the Eastern US, our analyses suggest that the apparent EF-precipitation coupling takes place on a short day-to-day time scale and is either atmospherically controlled (from precipitation persistence and potential evaporation) or driven by vegetation interception and subsequent re-evaporation (rather than soil moisture and related plant transpiration/bare soil evaporation), in line with the high forest cover and the wet regime of that region. Over the Central and Southwestern US, the impact of EF on convection triggering is additionally linked to soil moisture variations, owing to the soil moisture-limited climate regime.

Land surface controls on afternoon precipitation

B. P. Guillod et al.

Title Page

Abstract

Introduction

Conclusions

References

Tables

Figures



Back

Close

Full Screen / Esc

Printer-friendly Version

Interactive Discussion



1 Introduction

Soil moisture–precipitation feedback has been investigated for several decades and, despite some progress in recent years, remains a poorly understood process and a large source of uncertainty in climate models (Seneviratne et al., 2010). While studies until the 1990s tended to focus on the concept of soil moisture recycling (i.e. the fraction of precipitation that is directly contributed by regional evaporation from the land, see Seneviratne et al., 2010), more recent studies have emphasized the importance of indirect feedback mechanisms, that is, an influence of soil moisture on atmospheric stability, boundary layer characteristics, and thereby precipitation formation (e.g. Schär et al., 1999; Pal and Eltahir, 2001; Findell and Eltahir, 2003a; Ek and Holtslag, 2004; Betts, 2004; Santanello et al., 2009; Hohenegger et al., 2009; Taylor et al., 2011; Lintner et al., 2013; Gentine et al., 2013). This indirect effect can theoretically lead to feedbacks of either sign (Seneviratne et al., 2010). For instance, over wet soils, humidity input into the boundary layer increases, but turbulence and boundary layer height decrease; the interplay of these two effects with the environment can trigger or suppress convection locally depending on the prevailing conditions (e.g., Ek and Holtslag, 2004; Gentine et al., 2013). Although most studies report a positive feedback, some suggest the existence of a negative feedback in certain regions (Findell and Eltahir, 2003a, b; Cook et al., 2006; Hohenegger et al., 2009; Westra et al., 2012; Gentine et al., 2013). Furthermore, non-local processes can also be important (e.g. Taylor and Ellis, 2006). In particular, spatial heterogeneity of soil moisture has been shown to induce mesoscale circulations favoring precipitation over dry soils, for example in the Sahel region (Taylor et al., 2011) but also globally (Taylor et al., 2012).

The entire soil moisture-precipitation feedback can be decomposed into a chain of processes as follows (Fig. 1, modified from Seneviratne et al., 2010):

- A. Soil moisture impacts the partitioning of energy at the land surface into sensible and latent heat flux (H and λE , respectively), as quantified by the evaporative fraction $EF = \frac{\lambda E}{H + \lambda E}$.

Land surface controls on afternoon precipitation

B. P. Guillod et al.

Title Page

Abstract

Introduction

Conclusions

References

Tables

Figures



Back

Close

Full Screen / Esc

Printer-friendly Version

Interactive Discussion



ger et al., 2009). Dirmeyer et al. (2006) highlight large biases in Global Climate Models (GCMs) with respect to covariability between key atmospheric and land-surface variables and Koster et al. (2003) suggest that soil moisture-precipitation feedbacks may be overestimated in GCMs.

5 Given the large range of results from modeling studies, observational studies are necessary. However, for a number of reasons, these have been largely inconclusive (Seneviratne et al., 2010). First, the scarcity of soil moisture and EF measurements is a recurrent limitation. In particular, while recent satellite remote-sensing efforts have allowed for global analyses leading to new findings (e.g. Taylor et al., 2012), these only
10 provide data on soil moisture in the top few centimeters of the soil and in regions without dense vegetation cover. This is often not representative of deeper layers and, thus, of EF, especially in vegetated areas. Second, we note that one of the most challenging tasks in assessing soil moisture-precipitation coupling (i.e., A-B) from observational data is to establish causal rather than mere statistical links between soil moisture (or
15 EF) and precipitation (see also Salvucci et al., 2002; Orłowsky and Seneviratne, 2010).

The difficulty of causal inferences from observational data arises from two main confounding effects. First, given the influence of precipitation on soil moisture (process C) it can be difficult to assess whether a detected relationship between soil moisture and precipitation is due to A-B, C or both. In particular, persistence in precipitation
20 at various time scales (from synoptic to interannual scales, including seasonal-scale) can induce apparent causal links, for which even lagged correlations between e.g. soil moisture and subsequent precipitation may in fact simply reflect relationship C. Second, covariability between two variables (for instance soil moisture and convective precipitation) may be a necessary but not a sufficient condition for a causal link since it
25 does not exclude the possibility that both quantities are governed by a third influencing variable (for instance sea surface temperature, see Orłowsky and Seneviratne, 2010). Ideally, potential confounding variables should be taken into account in observational analyses; this is, however, rarely done in practice, mostly due to difficulties in identifying confounding variables or lack of data availability.

Land surface controls on afternoon precipitation

B. P. Guillod et al.

Title Page

Abstract

Introduction

Conclusions

References

Tables

Figures



Back

Close

Full Screen / Esc

Printer-friendly Version

Interactive Discussion



**Land surface
controls on afternoon
precipitation**B. P. Guillod et al.

[Title Page](#)[Abstract](#)[Introduction](#)[Conclusions](#)[References](#)[Tables](#)[Figures](#)[◀](#)[▶](#)[◀](#)[▶](#)[Back](#)[Close](#)[Full Screen / Esc](#)[Printer-friendly Version](#)[Interactive Discussion](#)

In order to overcome the issue of data scarcity, some studies have made use of state-of-the-art reanalysis products (e.g. Bisselink and Dolman, 2008; Findell et al., 2011). Soil moisture and associated land-surface fluxes in reanalysis products are, however, ultimately model-based and therefore share the deficiencies of their land-surface models. Some reanalysis products assimilate screen-level variables (temperature, humidity) in order to better constrain the surface energy budget (Mahfouf, 1991; Bouttier et al., 1993b, a; Gentine et al., 2011) and may thus be advantageous over other reanalysis products. Nonetheless, such land data assimilation procedures may introduce biases in surface variables (e.g. Betts et al., 2003; Seneviratne et al., 2004). In addition, reanalyses suffer from other issues such as the lack of mass conservation. Therefore, reanalyses-based investigations are a useful complement to but ultimately cannot replace observational studies. Finally, they suffer from the similar difficulties in isolating causal relationships as the studies based on observational data, although they provide a more comprehensive data basis.

In this study, we investigate soil moisture–EF–precipitation coupling (i.e., processes A and B) over North America, addressing the aforementioned issues. We use direct observations of EF and precipitation from FLUXNET sites, remote-sensing-derived products (satellite-based EF from GLEAM and precipitation from the US radar network NEXRAD), and the North American Regional Reanalysis, NARR (see Sect. 2). Specifically, we quantify the effect of before-noon EF (and soil moisture) on afternoon convective rainfall occurrence via the Triggering Feedback Strength (TFS, see Findell et al., 2011 and Sect. 3). This metric suggests, when applied to NARR, a region of coupling over the Eastern US (Findell et al., 2011). Here, we first compare TFS estimates derived from observation-based datasets with that from NARR (Sect. 4). We then analyze the potential confounding effect of precipitation persistence on TFS (Sect. 5), and further investigate the role of soil moisture and vegetation interception storage on land evaporation and the inferred EF-precipitation coupling (Sect. 6). Finally, results from these sections and their implications are discussed in Sect. 7.

2 Datasets

We provide here a description of the datasets used in this study. The analysis is restricted to North America for consistency with Findell et al. (2011). The datasets considered here include a reanalysis product (the North American Regional Reanalysis, hereafter referred to as NARR), ground-based point-scale observations from FLUXNET, and remote-sensing-derived products: the NEXt generation weather RADar system (NEXRAD) and Global Land Evaporation: the Amsterdam Methodology (GLEAM). They are summarized in Table 1. For three-hourly datasets (NARR and GLEAM), values closest to local 3 h (in standard local time based on longitude) are used, as in Findell et al. (2011). Thus, a lag of up to one hour between datasets can occur in either direction, depending on the longitude.

2.1 NARR

The North American Regional Reanalysis (NARR, see Mesinger et al., 2006) is maintained at the National Center for Environmental Prediction (NCEP) and spans the period from 1979 to present. With its high spatial (about 32 km horizontal) and temporal (3 h) resolution, it allows for analyses focused on the diurnal evolution of land-atmosphere variables, which is an important aspect when analyzing the impact of surface fluxes on convection and precipitation. Its key characteristic is that it successfully assimilates high-quality precipitation observations into the atmospheric analysis, contrary to other reanalyses. Thus, since it forces the land-surface model component of the system more accurately than in other reanalyses, it may allow for more realistic analyses of land hydrology and land-atmosphere interactions. However, an in-situ comparison to observational data shows that surface radiation fluxes can be significantly biased in NARR (Kennedy et al., 2011). Moreover, West et al. (2007) identified spurious grid-scale precipitation events and related them to anomalous latent heating in cases of strong mismatch between assimilated and modeled precipitation. Also of high relevance in the context of EF-precipitation coupling analyses, Ruane (2010a, b) high-

Title Page

Abstract

Introduction

Conclusions

References

Tables

Figures



Back

Close

Full Screen / Esc

Printer-friendly Version

Interactive Discussion



area, possible change in footprint depending on e.g. wind direction), provides largely model-independent data and is therefore a direct estimate pertinent to our analyses.

In this study, we use data from the FLUXNET LaThuile dataset, a global standardized database of eddy covariance measurements which includes a large number of sites.

5 Measurements of sensible (H) and latent (λE) heat fluxes are used to compute EF, while global radiation (i.e., incoming shortwave, R_g) and potential global radiation (i.e. extraterrestrial radiation, R_g^{pot}) are used to get a proxy for cloud cover (see Sect. 3.2). One of the main issues with eddy-covariance measurements is that the energy balance is not closed, likely due to an underestimation of H and λE (e.g. Wilson et al., 2002; 10 Foken, 2008; Hendricks Franssen et al., 2010). However, as we do not use H and λE directly but only through EF, we note that the commonly used “fixed Bowen ratio” correction for the energy balance closure (i.e. attributing the missing energy to latent and sensible heat fluxes while keeping the Bowen ratio $B_w = \frac{H}{\lambda E}$ constant, e.g. Blanken et al., 1997) does not affect EF. Hence, we can expect that EF is only marginally af- 15 fected by the mentioned measurement error at the sites.

A total of 39 sites, listed in Table 2, are used in this study, all of them located in the US and Canada. The selection of the sites is based on several criteria: first, coverage by precipitation radars from NEXRAD (see Sect. 2.3) as well as R_g measurements are requirements for use in our study. Second, summers with many gaps in any of the 20 required variables are removed, and only sites with a reasonable amount of remaining data are kept for the analysis ($\gtrsim 100$ days).

2.3 NEXRAD

The NEXt generation weather RADar system (NEXRAD) is a network of 159 Weather Surveillance Radar-1988 Doppler (WSR-88D) sites covering the United States. Data 25 are archived at the National Climatic Data Center (NCDC) of the US National Weather Service. Here, we use the one-hour precipitation product (N1P) from the level III data. More details about NEXRAD products can be found at <http://www.ncdc.noaa.gov/oa/>

Land surface controls on afternoon precipitation

B. P. Guillod et al.

Title Page

Abstract

Introduction

Conclusions

References

Tables

Figures

◀

▶

◀

▶

Back

Close

Full Screen / Esc

Printer-friendly Version

Interactive Discussion



radar/radarresources.html (accessed on 20 December 2012). N1P data for summer (June to August, JJA) from 1995 to 2007 were downloaded at NEXRAD stations covering FLUXNET sites and their vicinity. We use 3 h averages of precipitation within 20 km around each FLUXNET site. Aggregating with different radii and time-averaging methods leads to robust results (not shown).

2.4 GLEAM

GLEAM (Global Land Evaporation: the Amsterdam Methodology – see Miralles et al., 2011b) is a global dataset of daily land-surface evaporation (E) based on satellite observations, available at a resolution of 0.25° . Estimates of E for day i are derived based on:

$$E_i = E_i^{\text{pot}} S_i + (1 - \beta) I_i \quad (1)$$

where E_i^{pot} is the potential evaporation (at day i), derived through the Priestley and Taylor formulation (Priestley and Taylor, 1972) using data of net radiation (R^{net}) and near-surface air temperature. S_i denotes the evaporative stress (at day i) and is computed combining (a) observations of vegetation water content (microwave vegetation optical depth) and (b) estimates of root-zone soil moisture (θ_i) from a multi-layer soil module driven by observations of precipitation (P_i) and surface soil moisture (θ_i^{obs}). The inclusion of vegetation optical depth accounts for the effects of plant phenology; its low day-to-day variability causes minor effects on the short-term dynamics of E_i . I_i denotes the vegetation rainfall interception loss, calculated based on Gash's analytical model of rainfall interception (Gash, 1979) and described in detail by Miralles et al. (2010); β is a constant to account for declines in transpiration when the canopy is wet – for more details see Miralles et al. (2010, 2011b).

We use a version of GLEAM that is driven by the input datasets noted in Table 3; importantly, precipitation from NEXRAD (see Sect. 2.3) is used to estimate interception loss and drive the soil module. GLEAM usually operates at daily time steps due

Land surface controls on afternoon precipitation

B. P. Guillod et al.

Title Page

Abstract

Introduction

Conclusions

References

Tables

Figures

◀

▶

◀

▶

Back

Close

Full Screen / Esc

Printer-friendly Version

Interactive Discussion



Land surface controls on afternoon precipitation

B. P. Guillod et al.

Title Page

Abstract

Introduction

Conclusions

References

Tables

Figures

◀

▶

◀

▶

Back

Close

Full Screen / Esc

Printer-friendly Version

Interactive Discussion



to assumptions underlying the conductivity of water in the soil module and Gash's analytical model of interception. Here, to estimate before-noon EF (9 a.m.–12 p.m., i.e. $EF_{i,9-12}$) several modifications to the original methodology are undertaken. As shown in Eq. (1), the computation of E_i requires daily estimates of potential evaporation, E_i^{pot} , evaporative stress, S_i , and interception, I_i . GLEAM daily input variables are aggregated to represent a diurnal cycle beginning/ending at around 9 a.m. standard local time. Therefore, the estimates of root-zone soil moisture (θ_{i-1}) used to derive S_{i-1} , roughly correspond to 9 a.m. on day i , as they are derived using the cumulative precipitation up to 9 a.m. and instantaneous observations of surface soil moisture from the early morning hours (between 1.30 a.m. and 6 a.m. depending on the satellite platform – see Owe et al., 2008, for details on the soil moisture remote-sensing product).

Thereby, for our calculations of GLEAM's before-noon EF at day i (i.e., $EF_{i,9-12}$), we use S_{i-1} as a proxy for the evaporative stress conditions. Since days with morning-time precipitation are not included in the computations of the TFS, $I_{i,9-12}$ is assumed to be zero. $EF_{i,9-12}$ is therefore calculated as:

$$EF_{i,9-12} = \frac{\lambda E_{i,9-12}^{\text{pot}} S_{i-1}}{R_{i,9-12}^{\text{net}} - G_{i,9-12}} \quad (2)$$

where R^{net} is net radiation from the GEWEX SRB dataset (satellite-based product, see Stackhouse et al., 2004) and G is the ground heat flux, computed as a function of R^{net} and land cover type as by Miralles et al. (2011b).

In this form, S_{i-1} accounts for evaporative stress due to soil moisture deficits only. This is not accurate if vegetation stores intercepted water from the previous-day precipitation. We therefore use a modified version, S_{i-1}^* , which assumes that water remains on vegetation from the previous-day precipitation and that the vaporization of this water is powered by radiation (i.e., interception loss is a fraction of the radiation-based Priestley and Taylor potential evaporation). Hence, we can re-arrange Eq. (1) as

$E_i = E_i^{\text{pot}} S_i + (1 - \beta) I_i = E_i^{\text{pot}} S_i^*$, which yields

$$S_{i-1}^* = S_{i-1} + (1 - \beta) \frac{I_{i-1}}{E_{i-1}^{\text{pot}}}. \quad (3)$$

Estimates of $EF_{i,9-12}$ are then computed using S_{i-1}^* instead of S_{i-1} in Eq. (2), and therefore include the effect of interception.

Note that this implies a revision of the standard GLEAM framework, in which interception loss is not limited by local net radiation (see e.g. Holwerda et al., 2012).

To summarize, $EF_{i,9-12}$ is computed in three steps:

1. GLEAM is first run as in Miralles et al. (2011b) to derive the daily averages of evaporation (E_i) and evaporative stress (S_i) – see Eq. (1). The only difference here is that we compute daily values from about 9–9 a.m. for all variables (depending on longitude but always before 9 a.m.).
2. The evaporative stress S_i is recalculated as S_i^* using Eq. (3) to consider the effect of interception loss.
3. S_{i-1}^* is used to calculate before-noon EF (i.e. $EF_{i,9-12}$) using Eq. (2) (except in the left panel of Fig. 11, where S_{i-1} is used instead of S_{i-1}^* to isolate the effect of soil moisture).

Note that the timing of the input datasets for the S and S^* computation is crucial to this application, in particular for precipitation. First, we do not want to include any information about afternoon precipitation for the estimated before-noon EF on the same day. Second, rainfall occurring in the night preceding the estimated EF must be included in order to get an EF reflecting the conditions in the early morning. Unfortunately, the definition of “days” in many standard daily precipitation products varies, as shown in Table S1 in the Supplement, and is sometimes unclear: for instance, the use of data from the Global Precipitation Climatology Project (GPCP, see Huffman et al., 2001) is

Land surface controls on afternoon precipitation

B. P. Guillod et al.

Title Page

Abstract

Introduction

Conclusions

References

Tables

Figures

◀

▶

◀

▶

Back

Close

Full Screen / Esc

Printer-friendly Version

Interactive Discussion



**Land surface
controls on afternoon
precipitation**B. P. Guillod et al.

[Title Page](#)[Abstract](#)[Introduction](#)[Conclusions](#)[References](#)[Tables](#)[Figures](#)[⏪](#)[⏩](#)[◀](#)[▶](#)[Back](#)[Close](#)[Full Screen / Esc](#)[Printer-friendly Version](#)[Interactive Discussion](#)

inappropriate due to the time window of the dataset (0:00 to 0:00 UTC, i.e. from 4 p.m. (7 p.m.) to 4 p.m. (7 p.m.) in the US West (East) Coast, see Table S1). Also noteworthy, for the CPC Unified gauge product (Chen et al., 2008) days are defined differently depending on the country. For most of the USA, the defined window is 12:00 to 12:00 (UTC, i.e. 4–4 a.m. in the West Coast/8–8 a.m. in the East Coast), which in principle suits our requirements although uncertainties remain due to differing reporting times between contributing rain gauge stations. NEXRAD is not affected by this issue given its higher temporal resolution.

Given the large range of precipitation products, the sensitivity of GLEAM to the precipitation dataset used as an input to derive EF time series has been investigated in the Supplement (see Supplement Discussion S2). Datasets used for this sensitivity test are NEXRAD, CPC-Unified (Chen et al., 2008) and PERSIANN (Hsu et al., 1997). These three datasets either suit the required daily time window (like in the case of CPC-Unified) or have a sub-daily temporal resolution and therefore appropriate daily aggregates can be constructed (like in the case of NEXRAD and PERSIANN). With the exception of three sites in the middle of the Western US, where NEXRAD data displays suspect features, results obtained from these three independent precipitation datasets are qualitatively similar (see Fig. S3 and text in the Supplement for more details).

3 Methods

This section provides details on the convection triggering metric TFS, including the selection of potentially convective days to which the computations are restricted, and the statistical test for assessing the significance of the results.

3.1 Triggering Feedback Strength (TFS)

The TFS, defined by Findell et al. (2011), quantifies the link between before-noon EF and afternoon precipitation occurrence as

$$\text{TFS} = \sigma_{\text{EF}} \frac{\partial \Gamma(r)}{\partial \text{EF}} \quad (4)$$

where EF is the before-noon evaporative fraction (computed between 9 a.m.–12 p.m. where 12 p.m. is noon), σ_{EF} is the standard deviation of EF and $\Gamma(r)$ is the probability of afternoon rain (> 1 mm, computed between 12–6 p.m.). The computation is restricted to summer days (June to August, JJA). In addition, only potentially convective days are included in the computation in order to reduce the impact of large-scale synoptic systems and thus to restrict the analysis to days when surface turbulent fluxes of sensible and latent heat are most likely to impact precipitation formation (see Sect. 3.2). It should be noted that, like most statistical analyses, a high TFS does not necessarily imply causality between $\Gamma(r)$ and EF, but simply the existence of a correlation between the two variables.

Findell et al. (2011) compute TFS in bins of the parameter space of EF, CTP and HI_{low} (the Convective Triggering Potential and a low-level Humidity Index, respectively; see Findell and Eltahir, 2003a), which are subsequently aggregated. This is done in order to reduce possible confounding effects from these variables. In our study, however, relatively short observational time series preclude extensive sampling of this parameter space and independent observational sources for CTP and HI_{low} , i.e. radio soundings, do not exist in the vicinity of all analyzed FLUXNET sites.

We can therefore only approximate the approach of Findell et al. (2011). Thus, we compute here a simplified version of TFS,

$$\text{TFS}^* = \sigma_{\text{EF}} \frac{\Gamma(r|\text{EF} > \text{EF}_{\text{Q60}}) - \Gamma(r|\text{EF} \leq \text{EF}_{\text{Q40}})}{\text{EF}_{\text{Q80}} - \text{EF}_{\text{Q20}}}, \quad (5)$$

Land surface controls on afternoon precipitation

B. P. Guillod et al.

Title Page

Abstract

Introduction

Conclusions

References

Tables

Figures

◀

▶

◀

▶

Back

Close

Full Screen / Esc

Printer-friendly Version

Interactive Discussion



where EF_{Q_X} is the X th percentile of EF. The variable σ_{EF} and the percentiles of EF are determined for each location and dataset independently. The definition of the bins ensures clearly distinct bins (i.e. no possible overlap even if $EF_{Q_{60}} = EF_{Q_{40}}$) while retaining most of the available data. Considering quantiles also partly accounts for different shapes of the EF distributions when comparing different EF datasets. EF values outside of the 0–1 range are excluded from the analysis. Although TFS* is an approximation of the original TFS defined by Findell et al. (2011), the two different computations show close agreement when applied to NARR (see Supplement).

3.2 Identification of potentially convective days

Typical convective situations differ from synoptic weather systems in the physical processes involved and can be, to some extent, identified using different variables. In particular, convection tends to occur in the afternoon as a result of the day time boundary layer evolution (Rio et al., 2009). Potentially convective days are therefore expected to be rain- and cloud-free in the morning. Moreover, convection is usually linked to low atmospheric stability and, therefore, typically positive CTP. Based on these observations, sets of criteria to select potentially convective days to be included in the TFS* computation can be defined to remove impacts of large-scale, persistent synoptic weather systems.

Findell et al. (2011) identify potentially convective days as days with $CTP > 0$ and no morning precipitation. However, in the absence of the necessary information for CTP from observations, we alternatively use the following criteria throughout our analyses:

- No morning precipitation, as in Findell et al. (2011), and
- $R_g/R_g^{pot} > 0.67\max(R_g/R_g^{pot})$ in the morning, where R_g is the global radiation (i.e. incoming short-wave) at the land surface and R_g^{pot} is the potential R_g in the absence of atmosphere (i.e. extraterrestrial incoming short-wave).

Land surface controls on afternoon precipitation

B. P. Guillod et al.

Title Page

Abstract

Introduction

Conclusions

References

Tables

Figures

◀

▶

◀

▶

Back

Close

Full Screen / Esc

Printer-friendly Version

Interactive Discussion



R_g is available from NARR and measured at FLUXNET sites. R_g^{pot} being dependent on time and latitude only, it is computed for each grid cell used in our analysis for NARR, while it is readily available in FLUXNET data. The computation of $\max(R_g/R_g^{\text{pot}})$, restricted to summer days (JJA), is applied to each site to account for site-specific conditions. R_g/R_g^{pot} therefore quantifies the fraction of incoming solar radiation reaching the ground, and its maximum value corresponds to clear-sky cases. Requiring $R_g/R_g^{\text{pot}} > 0.67\max(R_g/R_g^{\text{pot}})$ in the morning is used to remove days with morning clouds from the analysis as they are likely linked to synoptic systems. Cutoff ratios between 0.5 and 0.8 do not lead to different results (not shown).

In this study, the dataset combinations use these criteria computed on the following datasets, chosen according to data availability:

- NARR: precipitation and R_g from NARR
- FLUXNET-NEXRAD: precipitation from NEXRAD and R_g from FLUXNET
- GLEAM-NEXRAD: precipitation from NEXRAD and R_g from NARR

The impact of the criteria for the selection of potentially convective days on TFS*, in particular with respect to the NARR analysis and the different set of criteria used in our study compared to Findell et al. (2011), is small, as discussed in the Supplement (Fig. S2).

3.3 Statistical tests

The statistical significance of $\text{TFS}^* \neq 0$ is tested by bootstrap samples. A TFS* distribution is computed from 1000 bootstrap samples for which the EF data are kept unchanged and precipitation data are shuffled, which simulates the null hypothesis that no relation between EF and precipitation exists. The bootstrap TFS* distribution is approximately symmetrical with respect to 0. For a 90 % significance level, we require a positive (negative) TFS* to be at or above (below) the 95 percentile (5 percentile).

We chose a rather low significance level of 90 % to account for the relatively short time series and the noise inherent in the data.

4 TFS from different datasets

The impact of before-noon EF on precipitation occurrence is quantified using the modified Triggering Feedback Strength TFS* (see Sect. 3). TFS* is computed at FLUXNET sites from three dataset combinations: (i) a reanalysis product (NARR), (ii) direct measurements of surface turbulent heat fluxes at FLUXNET sites for EF in combination with radar precipitation from NEXRAD, and (iii) a satellite-based estimation of EF (GLEAM) in combination with NEXRAD precipitation. We compare estimates of the Triggering Feedback Strength (TFS*) from these datasets (Sect. 4.1), complemented by comparing general characteristics of the EF datasets (Sect. 4.2).

4.1 Overview

Figure 2 displays TFS* computed at FLUXNET site locations for the three analyzed dataset combinations. Before comparing the results obtained with the different datasets, we note that the pattern obtained from NARR reproduces that of Findell et al. (2011) quite well, with a region of large significant TFS* values over the Eastern US. This shows that our simplified TFS* computation (Eq. 5) reproduces the more sophisticated computation from Findell et al. (2011). The impacts of the years included in the analysis and of different sets of criteria for the selection of potentially convective days are individually analyzed in the Supplement (Figs. S1 and S2, respectively) and turn out to be negligible.

To complement the maps shown in Fig. 2, the distributions of TFS* values for the three datasets are compared separately over three regions (Western, Central and Eastern US) using boxplots (Fig. 3). The definition of these regions is based on expected coupling regions from previous studies. The central US region represents a typical

Land surface controls on afternoon precipitation

B. P. Guillod et al.

Title Page

Abstract

Introduction

Conclusions

References

Tables

Figures

⏪

⏩

◀

▶

Back

Close

Full Screen / Esc

Printer-friendly Version

Interactive Discussion



soil moisture–precipitation coupling “hot spot” expected from other studies (e.g. Koster et al., 2004), while the Eastern US displays strong EF-precipitation positive relationship in NARR (Findell et al., 2011). The Western US, on the other hand, is a dry region (soil moisture limited regime, see Thomas et al., 2009; Schwalm et al., 2012) with little soil moisture and EF variability and is therefore usually not considered as being conducive to strong soil moisture–precipitation feedbacks. Strong EF-precipitation coupling (e.g. over the Eastern US in NARR) is a necessary but not sufficient condition for strong soil moisture-precipitation coupling.

Generally, FLUXNET displays large variations within each region (Fig. 3) and even within smaller climatic regions (e.g. in Florida, Fig. 2). Thus, it does not display much of the significant TFS* regional pattern evident in NARR over the Eastern US (Fig. 2). On the other hand, the remote-sensing estimate from GLEAM and NEXRAD yields some significant values in that region, although TFS* is generally smaller for this combination and not as consistently significant as in NARR. Over both the Central US and South-western US, GLEAM-NEXRAD and to some extent FLUXNET show larger TFS* values compared to NARR (Figs. 2 and 3). Results from GLEAM-NEXRAD for the three sites in the middle of the Western region indicated by empty dots on Fig. 3 (map), however, should be interpreted with caution, as inspection of the NEXRAD time series reveals suspect features in some years (not shown). Note that GLEAM data generated with input from three independent precipitation datasets lead to similar results, albeit with less consistent TFS* in the Eastern US (Sect. 2.4 and Supplement and Fig. S3), except for the three mentioned sites in the middle of the Western US with issues in NEXRAD and for which only GLEAM generated with NEXRAD displays strong coupling in the Western US.

Several reasons might contribute to the observed differences between TFS* estimates from the different datasets:

- i. Spatial scale of the EF data: the footprint of FLUXNET measurements is much smaller than the grid cells of NARR and GLEAM (typically 100–2000 m vs about 25–30 km, respectively, see Sect. 4.2). In Fig. 4, which displays TFS* for the dif-

Land surface controls on afternoon precipitation

B. P. Guillod et al.

Title Page

Abstract

Introduction

Conclusions

References

Tables

Figures



Back

Close

Full Screen / Esc

Printer-friendly Version

Interactive Discussion



Land surface controls on afternoon precipitation

B. P. Guillod et al.

[Title Page](#)[Abstract](#)[Introduction](#)[Conclusions](#)[References](#)[Tables](#)[Figures](#)[⏪](#)[⏩](#)[◀](#)[▶](#)[Back](#)[Close](#)[Full Screen / Esc](#)[Printer-friendly Version](#)[Interactive Discussion](#)

most sites and across all dataset combinations. This suggests that the disagreement between the TFS* patterns in different dataset combinations is related to differences in the considered EF datasets (see also Fig. 4). Correlations of 10 day and monthly averages of before-noon EF are slightly higher but remain low (Fig. S4 in the Supplement). Correlations of EF anomalies (i.e. after removing the seasonal cycle within JJA) instead of actual values display similar results (not shown).

Several reasons might underlie the differences in EF datasets. First, the spatial scale over which EF is estimated, or footprint, is different for each dataset. Measurements from FLUXNET are local, with a footprint typically extending from 100–2000 m (Schmid, 1994), while NARR and GLEAM estimate EF over a much larger scale (about 0.3° and 0.25° , respectively). Differences might thus arise from different environmental conditions over the respective footprints (e.g., input of water from rainfall in case of very local precipitation events), but also from differences in land cover. Indeed, while wet vs. dry periods might be similar in all datasets, some studies have shown that different vegetation might respond differently to given conditions (Teuling et al., 2010). Land cover is in fact different at FLUXNET sites compared to the larger scale in NARR, in particular in regions with cultivated land, as FLUXNET sites are often located over natural vegetation. However, we did not find any systematic link between different land covers and resulting TFS* (not shown). Similarly, soil texture impacts soil moisture dynamics and EF (e.g. Guillod et al., 2013) and differences in local vs. larger scale soil texture could also be a reason for the differences in EF.

In order to better characterize the EF time series, Fig. 6 shows the mean, standard deviation, and persistence (quantified by the decorrelation time-scale, τ_D , which integrates the autocorrelation function, see von Storch and Zwiers, 1999) of EF for the three analyzed datasets. While we do not find any clear differences between the datasets that can explain the resulting differences in TFS*, the comparison highlights some interesting features. The mean EF is similar in all datasets and exhibits higher values in the Eastern US (wetter climate) compared to the drier climate of the Western US. This pattern is slightly stronger in GLEAM, where the Eastern US display higher

mean EF values than in other datasets. The EF standard deviation is noisy, although similar patterns are found across all datasets, with higher EF variability in the Central US or in the Southern Great Plains (the exact location depending on the dataset). Note, however, that the amplitudes differ widely between datasets. This does not necessarily impact TFS*: the change in the probability of afternoon precipitation with respect to EF is scaled by the standard deviation of EF (see Eq. 4 and Berg et al., 2013). Finally, EF persistence is generally lower in the Eastern US, suggesting high variability at a scale of one to a few days in this region of strong relationship in NARR (Fig. 2, left). Thus, the regions of strong daily correlation between EF and convection triggering correspond, in NARR, to humid regions with low persistence, while in GLEAM-NEXRAD the drier Western region, with higher persistence, displays strongest coupling.

5 Impact of EF vs precipitation persistence

Although the TFS metric is a useful tool for investigating the relationship between EF and convective precipitation triggering, precipitation persistence might lead to high TFS even in the absence of an actual impact of EF on precipitation. Indeed, as precipitation impacts soil moisture and thus EF, if precipitation events tend to be clustered together they will lead to high EF during precipitation clusters, and low EF during clusters of days without precipitation. Thus, TFS will be high in that case simply because of precipitation persistence. Although one cannot exclude the possibility that precipitation days cluster together due to a feedback mechanism, this is more likely due to an atmospheric forcing favoring clustered precipitation days. Precipitation persistence might also arise from seasonality in precipitation; however, this effect is less relevant for our study as only summer is considered.

The filters for potentially convective days as well as the binning in CTP and HI_{low} categories in the TFS computation should ideally account for such confounding effects (see Sect. 3.2). Nevertheless, we specifically test for the effect of precipitation persistence on TFS* by replacing before-noon EF with precipitation from the previ-

Land surface controls on afternoon precipitation

B. P. Guillod et al.

Title Page

Abstract

Introduction

Conclusions

References

Tables

Figures



Back

Close

Full Screen / Esc

Printer-friendly Version

Interactive Discussion



Land surface controls on afternoon precipitation

B. P. Guillod et al.

Title Page

Abstract

Introduction

Conclusions

References

Tables

Figures

◀

▶

◀

▶

Back

Close

Full Screen / Esc

Printer-friendly Version

Interactive Discussion



ous day in the TFS* computation. With respect to an explanatory variable X , we denote the change in the probability of afternoon precipitation for high vs. low X as $\Delta\Gamma(X) = \Gamma(r|X > X_{Q60}) - \Gamma(r|X \leq X_{Q40})$. Figure 7 (left) shows $\Delta\Gamma(\text{EF})$ and $\Delta\Gamma(P_{d,\text{prev}})$ for NARR and the GLEAM-NEXRAD combination, where $P_{d,\text{prev}}$ is the precipitation on the previous day (in other words, EF is simply replaced by the daily precipitation from the previous day). Due to short record length, FLUXNET is omitted from this analysis. Note that the patterns of $\Delta\Gamma(\text{EF})$ strongly resemble the patterns of TFS* for these two dataset combinations (Fig. 2) as it is the term that leads to most of the TFS* signal: in Eq. (4), σ_{EF} and ∂EF mostly compensate each other. In addition, maps of σ_{EF} (Fig. 6) do not display a pattern similar to that of TFS* (Fig. 2). Using $\Delta\Gamma(X)$ allows for a direct comparison between the impact of EF and that of previous day precipitation, shown on the right of Fig. 7 as $\Delta\Gamma(P_{d,\text{prev}})$. In fact, previous day precipitation is a better predictor for afternoon precipitation occurrence than before-noon EF, which holds for both datasets and across all regions. Given these results, one can wonder if the signal with EF is, in fact, only reflecting precipitation persistence or if EF conveys additional information that can help explain afternoon precipitation.

In order to disentangle the impact of EF on precipitation from precipitation persistence, we apply a framework similar to Salvucci et al. (2002) to stratify the data based on previous day precipitation. Here, only the occurrence of precipitation is considered and we investigate whether the signal emerging with EF reflects previous day precipitation occurrence alone and thus may be an artifact of precipitation persistence on a short time-scale. Note that Salvucci et al. (2002) also accounted for seasonal-scale persistence by including a precipitation wetness index. We do not include such a term since our analysis is restricted to summer months; in addition, our aim is simply to account for precipitation persistence on a short time scale to exclude the impact of persisting large-scale events (e.g. fronts). Figure 8 shows TFS* independent of previous day precipitation (i.e., as shown before; left column) as well as conditioned on the occurrence of precipitation the day before: here TFS* is computed using days either without or with previous day precipitation (center and right columns, respectively). Note that the sub-

set without previous day precipitation additionally filters out precipitation clusters. Since the conditioning reduces the number of days available, this analysis is applied to NARR and GLEAM-NEXRAD but also to the longer set of NARR data, covering 1979–2007 (bottom row).

For both NARR and the GLEAM-NEXRAD combination, the signal over the Eastern US strongly weakens when days are conditioned on previous day rainfall (Fig. 8). This suggests an important role of precipitation persistence on subsequent precipitation and thus on TFS*. Note, however, that the length of the time series, shortened after filtering days based on previous day precipitation, might also impact the results: using all available years from NARR (1979–2007, bottom row), TFS* remains significant for days following precipitation events, where EF might provide information on afternoon precipitation that is additional to previous day precipitation occurrence. Nonetheless, for days following rainfree days the clear weakening of the signal suggests a possible strong role of precipitation persistence. In addition, persistence is part of the TFS* signal, which is stronger on days with precipitation on the previous day than on days following rain-free days. This could be due to events lasting a large number of days, leading to very wet conditions and high EF with precipitation likely to occur again, relative to shorter events (1–2 days) that might exhibit lower EF and no further precipitation. Over the Southwestern US, the signal is less sensitive to precipitation persistence and TFS* remains significant over most sites for both datasets.

Overall, precipitation persistence plays an important role and thereby affects TFS* in all datasets. Several factors can lead to high precipitation persistence, such as SST forcing e.g. linked with large-scale teleconnection patterns. In addition, we cannot exclude at least a partial contribution of EF-precipitation coupling to the identified persistence features, although higher correlation with previous-day precipitation than EF suggest that this is not the dominant mechanism. Conversely, the EF-precipitation relationship could either reflect atmospheric persistence, an actually existing EF-precipitation coupling, or a combination of both, none of which can be fully excluded.

Land surface controls on afternoon precipitation

B. P. Guillod et al.

Title Page

Abstract Introduction

Conclusions References

Tables Figures

◀ ▶

◀ ▶

Back Close

Full Screen / Esc

Printer-friendly Version

Interactive Discussion



combine and act together on EF, which can impact precipitation. While the distinction between these three components has to our knowledge rarely been discussed in the literature in the context of EF-precipitation coupling or soil moisture-precipitation feedback (with rare exceptions, e.g. by Savenije, 1995b, 2004 in the context of moisture recycling and Scott et al., 1997, 1995 in the context of precipitation persistence), it is of high relevance for the results presented here.

In order to investigate the role of the components of λE in the analyzed relationships, we compute $\Delta\Gamma(X)$ using NARR data where X is the water storage term controlling each component instead of EF, as was done with previous day precipitation in Fig. 7. Storage terms are used instead of individual fluxes, which are not available from NARR output. Figure 10a–d displays $\Delta\Gamma$ in NARR computed with, from left to right, EF, surface soil moisture (for E_{soil}), root zone soil moisture (for E_{trans}), and vegetation interception storage (for E_i). All these variables are before-noon (9 a.m.–12 p.m.) values. The definition of surface and root zone soil moisture in NARR is provided in Sect. 2.1.

Over the Eastern US, most of the $\Delta\Gamma$ signal found with EF in the Eastern US does not appear with soil moisture (for both surface or root zone soil moisture), apart from a significant signal over Florida with surface soil moisture. This suggests that the EF variability is not driven by soil moisture variations in this region. On the other hand, $\Delta\Gamma$ computed with vegetation interception storage displays a strong signal, suggesting that most of the signal with EF is linked to interception evaporation. Although this finding might appear surprising, note that the fraction of days with vegetation interception storage (Fig. 10g) amounts to roughly 15–35 % and is thus far from negligible, which is consistent with other studies (see e.g. Savenije, 2004; Gerrits and Savenije, 2011 for overviews on interception). However, this result is nuanced by Fig. 10e and f: $\Delta\Gamma(\text{EF})$ is not strongly sensitive to the exclusion of days with vegetation interception storage (Fig. 10e; Fig. 10f displays the difference to the computation including all days and is rather small). Since this remaining signal (Fig. 10e) cannot be attributed to vegetation interception, it is likely either due to one of the remaining terms of evaporation or to atmospheric controls on EF through potential evaporation. To test this hypothesis, the

Land surface controls on afternoon precipitation

B. P. Guillod et al.

Title Page

Abstract

Introduction

Conclusions

References

Tables

Figures

◀

▶

◀

▶

Back

Close

Full Screen / Esc

Printer-friendly Version

Interactive Discussion



Land surface controls on afternoon precipitation

B. P. Guillod et al.

Title Page

Abstract

Introduction

Conclusions

References

Tables

Figures

◀

▶

◀

▶

Back

Close

Full Screen / Esc

Printer-friendly Version

Interactive Discussion



third row of Fig. 10 displays $\Delta\Gamma(X)$ computed on days without vegetation interception and where X is, from left to right, surface soil moisture (Fig. 10h), root zone soil moisture (Fig. 10i), and potential EF ($EF_{\text{pot}} = \lambda E_{\text{pot}} / (R_n - G)$, i.e., the EF that corresponds to potential evaporation, Fig. 10j). For most of the Eastern US, EF_{pot} reproduces a substantial part of the signal while soil moisture (surface and root zone) does not. Thus, atmospheric controls on EF (through EF_{pot}) appear to play a dominant role.

Over other regions, we identify different key drivers based on Fig. 10. In Florida, surface soil moisture and vegetation interception explain best the observed signal with EF. Over the Southwestern US, our analysis highlights surface and root zone soil moisture as important contributors, with interception playing a smaller role. Over the Central US, no conclusion can be drawn from NARR as no EF–precipitation relationship is identified (see also Figs. 2 and 3).

The role of interception can also be investigated using GLEAM. In Fig. 11, we display TFS* for the GLEAM-NEXRAD combination as shown earlier (standard version, left) and when computing EF in GLEAM without including interception evaporation (right, see Eq. 2 in Sect. 2.4 for details on the computation). The significant positive TFS* signal over the Eastern US vanishes when interception is not accounted for. This shows that, for this observation-based dataset and over this region, interception is the main driver of the relationship between EF and subsequent precipitation, not soil moisture. Conversely, the large TFS* values found in the Central and Southwestern US remain significant after removing interception. Thus, in these regions, it is apparently soil moisture, and not interception, that leads to the observed coupling (not considering the three stations indicated on the map of Fig. 3 that exhibit issue in NEXRAD and that are further North in the Western US). This is consistent with the results from NARR over the Southwestern US.

Overall, analysis of the role of individual components of λE in the relationship between EF and subsequent precipitation leads to similar conclusions in NARR and in GLEAM-NEXRAD: in the Eastern US, the impacts of vegetation interception evaporation and environmental controls (such as entrainment) on EF lead to the observed

**Land surface
controls on afternoon
precipitation**B. P. Guillod et al.

[Title Page](#)[Abstract](#)[Introduction](#)[Conclusions](#)[References](#)[Tables](#)[Figures](#)[◀](#)[▶](#)[◀](#)[▶](#)[Back](#)[Close](#)[Full Screen / Esc](#)[Printer-friendly Version](#)[Interactive Discussion](#)

relationship. In the Central and Southwestern US, soil moisture (surface and root zone) drives the relationship, suggesting the likely occurrence of a soil moisture-precipitation feedback. These region-specific findings fit well with known regions of soil moisture-climate regimes and vegetation cover: Fig. 12a highlights a wet regime in the Eastern US, where land evaporation is controlled by radiation rather than soil moisture, unlike the soil moisture-limited regime of the Central and Western US. In addition, the Eastern US are mostly covered by forests, indicated by a high leaf area index in Fig. 12b, and thus vegetation interception is likely a relevant component of the evaporation over land in this region, unlike in the Southwestern US where vegetation cover is low and therefore vegetation interception is less relevant.

7 Discussion and conclusions

A recent study (Findell et al., 2011) statistically relates the occurrence of afternoon convective precipitation to before-noon Evaporative Fraction (EF) through the TFS metric (Triggering Feedback Strength), based on data from the North American Regional Reanalysis (NARR), and suggests the existence of an extended region of positive land surface–precipitation coupling over the Eastern US. Our study extends that analysis based on a systematic cross validation with additional independent, observation-based data sources and an in-depth investigation of all components contributing to the identified pattern from Findell et al. (2011).

We complement NARR with the use of observational data from FLUXNET stations (for EF) and from two remote-sensing-based products: GLEAM, an EF product derived based on satellite observations, and NEXRAD, the US network of ground-based precipitation radars. Factors that potentially influence the coupling quantification include model components that underlie reanalysis and remote-sensing products, different spatial scales of the FLUXNET and gridded data, time series lengths, precipitation persistence and interception evaporation. The next paragraphs summarize our findings.

investigated longer time scales. Although EF seems to provide a small additional predictability to precipitation alone in NARR, this result cannot be confidently confirmed with the GLEAM-NEXRAD combination, in particular in the Eastern US. Hence, the confounding impacts of precipitation on soil moisture and EF may preclude conclusions on the existence of a land-precipitation coupling in this region, as precipitation persistence could either be induced by a coupling or reflect the impact of large-scale forcings.

Accounting for the individual components of land evaporation (plant transpiration, bare soil evaporation and interception evaporation) in the analysis provides in-depth insight into the processes contributing to the observed patterns. Our results suggest that the coupling, if present, arises from distinct sources in different regions.

Over the Eastern US, atmospheric controls on EF (i.e., the atmospheric demand through potential evaporation) and vegetation interception drive the EF-precipitation relationship in NARR. The role of atmospheric controls on EF might indicate of relevance of large-scale controls on the observed relationship, consistently with the role of precipitation persistence, but identifying these drivers is beyond the scope of this study. This is also in line with work from Aires et al. (2013) who, using a neural network approach to analyze precipitation and to disentangle the impact of EF from those of other environmental factors, show that the latter (primarily HI_{low}) exert strong controls on precipitation. The positive relationship vanishes in the GLEAM-NEXRAD combination when interception evaporation is removed from the EF estimate, supporting the strong role of this component in this region. This is consistent with the high forest cover and the associated LAI in this region and it could further explain the lack of coupling from FLUXNET EF, since much of the interception evaporation is likely not captured by eddy-covariance measurements due to wet sensors (e.g. Mizutani et al., 1997). Although often neglected in the literature, we recall that evaporation from interception is a substantial part of land evaporation: it has been estimated to amount to 11 % of global land evaporation (Miralles et al., 2011a) and to an even larger proportion over forests (20–50 %, e.g. Savenije, 2004; McLaren et al., 2008; Gerrits and Savenije, 2011).

Land surface controls on afternoon precipitation

B. P. Guillod et al.

Title Page

Abstract

Introduction

Conclusions

References

Tables

Figures

◀

▶

◀

▶

Back

Close

Full Screen / Esc

Printer-friendly Version

Interactive Discussion



**Land surface
controls on afternoon
precipitation**

B. P. Guillod et al.

Title Page

Abstract

Introduction

Conclusions

References

Tables

Figures

◀

▶

◀

▶

Back

Close

Full Screen / Esc

Printer-friendly Version

Interactive Discussion



Although the strong role of vegetation interception in the coupling questions the classical interpretation of soil moisture affecting precipitation via EF, it is not totally surprising, given the large EF values in the identified regions, i.e., a humid regime with hardly any control of soil moisture on EF, unlike what has been diagnosed in several studies for the Central US (e.g. Koster et al., 2004; Teuling et al., 2009; Seneviratne et al., 2010). Thus, it is path 1 from Fig. 9 (C₁-A₁-B) which is mainly active in this wet, forested region – other components of land evaporation contribute to EF but not substantially to its variability and therefore not to the feedback. The thereby relatively short time-scale of the EF-precipitation relationship in this region is consistent with the role of day-to-day precipitation persistence. In fact, since precipitation of the previous day strongly impacts EF through vegetation interception, precipitation persistence could then be due either to an impact of EF (through interception) on precipitation or through atmospheric persistence – or the combination of both. Conversely, vegetation interception, being a good indicator of previous-day precipitation, could only be related to afternoon precipitation due to confounding effects of precipitation persistence. Distinguishing between these two possible mechanisms is difficult if not impossible, since precipitation and interception evaporation are directly linked with one another. Note here that with the selection of potentially convective days (Sect. 3.2), days with morning rainfall are excluded from all analyses. Interception therefore comes from rainfall on the preceding night or day.

The processes acting in the Central and Southwestern US are different than over the Eastern US. The lower leaf area index in these regions results in lower interception evaporation. Thus, the relationship between EF and precipitation occurrence found in GLEAM-NEXRAD, stronger than in the Eastern US, remains when interception evaporation is removed from the EF estimate, highlighting a likely impact of EF via soil moisture. Similarly in NARR, soil moisture is identified as the primary driver of the relationship at the few sites which exhibit significant TFS* in this dataset for these regions. This is consistent with the soil moisture-limited evaporation regime in this transitional region (Koster et al., 2004; Seneviratne et al., 2010; Mueller and Seneviratne, 2012) and

aligns well with expected regions of soil moisture–precipitation coupling (e.g. Koster et al., 2004). In addition, it fits well with the lower sensitivity of the signal to day-to-day precipitation persistence. Thus, from the schematic representation of Fig. 9, path 1 is expected to be of low relevance in that region. Path 3 is also likely less relevant than in the East since transpiration acts through vegetation, but we recall that grasslands and croplands cover large parts of the Central US and that transpiration can be higher over these vegetation types than over forests (see e.g. Teuling et al., 2010). Therefore, path 2, and path 3 where vegetation cover is high, are expected to dominate in these regions, leading to the impacts of soil moisture on EF found in GLEAM-NEXRAD and in NARR over the Southwestern US, and found in GLEAM-NEXRAD over the Central US. The lack of signal in NARR over the Central US while the GLEAM-NEXRAD combination displays some significant relationship suggests that some processes might be misrepresented in this reanalysis product, although issues in the other datasets cannot be excluded in spite of stronger observational components. Note that the Southwestern region is limited to the vicinity of the Mexican border and does not include sites at higher latitudes, where significant TFS* in GLEAM-NEXRAD is likely due to issues in NEXRAD.

In the analyses shown here, we divide the US into three large regions over which the processes are likely different due to different evaporation regimes. We note, however, that a number of other processes are not considered. In particular, one cannot exclude strong coupling gradients on scales much smaller than the sub-continental scales considered here. For instance, although in the dry region of the Northwestern US, evaporation is soil moisture-limited (e.g. Schwalm et al., 2012) but its variability is low, likely leading to low coupling with precipitation, this could further depend on local factors such as land cover (e.g. comparing young vs. mature forests, see Vickers et al., 2012). Moreover, in contrast to other US regions, the effects of orographic lifting of moist ocean air in the northwest can dominate over land–atmosphere interactions. The detailed analysis of these local features is, however, beyond the scope and spatial scale of our study.

Land surface controls on afternoon precipitation

B. P. Guillod et al.

Title Page

Abstract

Introduction

Conclusions

References

Tables

Figures

◀

▶

◀

▶

Back

Close

Full Screen / Esc

Printer-friendly Version

Interactive Discussion



forecasting (days), it is of limited use for climate forecasting. The identified region over the Eastern US might thus benefit from this new result for weather forecasts but likely not for climate simulations. However, the coupling found in the Central and Southwestern US, being linked to soil moisture with longer memory, is of high relevance for these two applications.

Given the large range of unresolved issues in the investigation of land–precipitation coupling, further studies are required to pin down this complicated relationship. Analyses of the feedback accounting for precipitation persistence and confounding variables, applied to different temporal and spatial scales and a wide range of datasets, are urgently needed. Simultaneously, improvements in models could possibly allow for more realistic sensitivity studies to tackle this issue. Finally, large-scale soil moisture and EF observations at scales relevant to land–atmosphere coupling (i.e., 10 km) would help provide additional observational constraints on model results.

Supplementary material related to this article is available online at
[http://www.atmos-chem-phys-discuss.net/13/29137/2013/
acpd-13-29137-2013-supplement.pdf](http://www.atmos-chem-phys-discuss.net/13/29137/2013/acpd-13-29137-2013-supplement.pdf).

Acknowledgements. We thank Han Dolman, Beverly E. Law, Altaf Alan, Markus Reichstein and Heini Wernli for discussions. The authors acknowledge the Swiss State Secretariat for Education and Research SER for funding under the framework of the COST Action ES0804. NARR data is provided by the NOAA/OAR/ESRL PSD, Boulder, Colorado, USA, from their Web site at <http://www.esrl.noaa.gov/psd/>. This work used eddy covariance data acquired by the FLUXNET community and in particular by the following networks: AmeriFlux (US Department of Energy, Biological and Environmental Research, Terrestrial Carbon Program (DE-FG02-04ER63917 and DE-FG02-04ER63911)) and Fluxnet-Canada (supported by CFCAS, NSERC, BIOCAP, Environment Canada, and NRCan). We acknowledge the financial support to the eddy covariance data harmonization provided by CarboEuropeIP, FAO-GTOS-TCO, iLEAPS, Max Planck Institute for Biogeochemistry, National Science Foundation, University of Tuscia, University Laval, Environment Canada and US Department of Energy and the database development and tech-

**Land surface
controls on afternoon
precipitation**

B. P. Guillod et al.

Title Page

Abstract

Introduction

Conclusions

References

Tables

Figures



Back

Close

Full Screen / Esc

Printer-friendly Version

Interactive Discussion



nical support from Berkeley Water Center, Lawrence Berkeley National Laboratory, Microsoft Research eScience, Oak Ridge National Laboratory, University of California – Berkeley and the University of Virginia.

References

- 5 Aires, F., Gentine, P., Findell, K., Lintner, B. R., and Kerr, C.: Neural network-based sensitivity analysis of summertime convection over the continental US, in review, 2013. 29167
- Angert, A., Barkan, E., Barnett, B., Brugnoli, E., Davidson, E. A., Fessenden, J., Maneepong, S., Panapitukkul, N., Randerson, J. T., Savage, K., Yakir, D., and Luz, B.: Contribution of soil respiration in tropical, temperate, and boreal forests to the ^{18}O enrichment of atmospheric O_2 , *Global Biogeochem. Cy.*, 17, 1089, doi:10.1029/2003GB002056, 2003. 29186
- 10 Baldocchi, D.: “Breathing” of the terrestrial biosphere: lessons learned from a global network of carbon dioxide flux measurement systems, *Aust. J. Bot.*, 56, 1–26, doi:10.1071/BT07151, 2008. 29145
- Baldocchi, D., Falge, E., Gu, L., Olson, R., Hollinger, D., Running, S., Anthoni, P., Bernhofer, C., Davis, K., Evans, R., Fuentes, J., Goldstein, A., Katul, G., Law, B., Lee, X., Malhi, Y., Meyers, T., Munger, W., Oechel, W., Paw, K. T., Pilegaard, K., Schmid, H. P., Valentini, R., Verma, S., Vesala, T., Wilson, K., and Wofsy, S.: FLUXNET: A new tool to study the temporal and spatial variability of ecosystem-scale carbon dioxide, water vapor, and energy flux densities, *B. Am. Meteorol. Soc.*, 82, 2415–2434, doi:10.1175/1520-0477(2001)082<2415:FANTTS>2.3.CO;2, 2001. 29145
- 20 Berg, A., Findell, K., Lintner, B. R., Gentine, P., and Kerr, C.: Precipitation sensitivity to surface heat fluxes over North America in reanalysis and model data, *J. Hydrometeorol.*, 14, 722–743, doi:10.1175/JHM-D-12-0111.1, 2013. 29159
- Betts, A. K.: Understanding hydrometeorology using global models, *B. Am. Meteorol. Soc.*, 85, 1673–1688, doi:10.1175/BAMS-85-11-1673, 2004. 29140
- 25 Betts, A. K., Ball, J. H., Bosilovich, M., Viterbo, P., Zhang, Y., and Rossow, W. B.: Intercomparison of water and energy budgets for five Mississippi subbasins between ECMWF reanalysis (ERA-40) and NASA Data Assimilation Office fvGCM for 1990–1999, *J. Geophys. Res.*, 108, 8618, doi:10.1029/2002JD003127, 2003. 29143

Land surface controls on afternoon precipitation

B. P. Guillod et al.

Title Page

Abstract

Introduction

Conclusions

References

Tables

Figures



Back

Close

Full Screen / Esc

Printer-friendly Version

Interactive Discussion



Land surface controls on afternoon precipitation

B. P. Guillod et al.

Title Page

Abstract

Introduction

Conclusions

References

Tables

Figures

◀

▶

◀

▶

Back

Close

Full Screen / Esc

Printer-friendly Version

Interactive Discussion



- Bisselink, B. and Dolman, A. J.: Precipitation recycling: moisture sources over Europe using ERA-40 Data, *J. Hydrometeorol.*, 9, 1073–1083, doi:10.1175/2008JHM962.1, 2008. 29143
- Blanken, P. D., Black, T. A., Yang, P. C., Neumann, H. H., Nesic, Z., Staebler, R., den Hartog, G., Novak, M. D., and Lee, X.: Energy balance and canopy conductance of a boreal aspen forest: partitioning overstory and understory components, *J. Geophys. Res.*, 102, 28915–28927, doi:10.1029/97JD00193, 1997. 29146
- Bo e, J.: Modulation of soil moisture-precipitation interactions over France by large scale circulation, *Clim. Dynam.*, 40, 875–892, doi:10.1007/s00382-012-1380-6, 2013. 29141
- Bouttier, F., Mahfouf, J.-F., and Noilhan, J.: Sequential assimilation of soil moisture from atmospheric low-level parameters, Part 2: Implementation in a mesoscale model, *J. Appl. Meteorol.*, 32, 1352–1364, doi:10.1175/1520-0450(1993)032<1352:SAOSMF>2.0.CO;2, 1993a. 29143
- Bouttier, F., Mahfouf, J.-F., and Noilhan, J.: Sequential assimilation of soil moisture from atmospheric low-level parameters, Part 1: Sensitivity and calibration studies, *J. Appl. Meteorol.*, 32, 1335–1351, doi:10.1175/1520-0450(1993)032<1335:SAOSMF>2.0.CO;2, 1993b. 29143
- Bracho, R., Starr, G., Gholz, H. L., Martin, T. A., Cropper, W. P., and Loescher, H. W.: Controls on carbon dynamics by ecosystem structure and climate for southeastern US slash pine plantations, *Ecol. Monogr.*, 82, 101–128, doi:10.1890/11-0587.1, 2011. 29187
- Chen, M., Shi, W., Xie, P., Silva, V. B. S., Kousky, V. E., Wayne Higgins, R., and Janowiak, J. E.: Assessing objective techniques for gauge-based analyses of global daily precipitation, *J. Geophys. Res.*, 113, D04110, doi:10.1029/2007JD009132, 2008. 29150
- Cook, B. D., Davis, K. J., Wang, W., Desai, A., Berger, B. W., Teclaw, R. M., Martin, J. G., Bolstad, P. V., Bakwin, P. S., Yi, C., and Heilman, W.: Carbon exchange and venting anomalies in an upland deciduous forest in northern Wisconsin, USA, *Agr. Forest Meteorol.*, 126, 271–295, doi:10.1016/j.agrformet.2004.06.008, 2004. 29187
- Cook, B. I., Bonan, G. B., and Levis, S.: Soil moisture feedbacks to precipitation in Southern Africa, *J. Climate*, 19, 4198–4206, doi:10.1175/JCLI3856.1, 2006. 29140, 29141
- Curtis, P. S., Hanson, P. J., Bolstad, P., Barford, C., Randolph, J., Schmid, H., and Wilson, K. B.: Biometric and eddy-covariance based estimates of annual carbon storage in five eastern North American deciduous forests, *Agr. Forest Meteorol.*, 113, 3–19, doi:10.1016/S0168-1923(02)00099-0, 2002. 29187

Land surface controls on afternoon precipitation

B. P. Guillod et al.

Title Page

Abstract

Introduction

Conclusions

References

Tables

Figures

◀

▶

◀

▶

Back

Close

Full Screen / Esc

Printer-friendly Version

Interactive Discussion



- Desai, A. R., Bolstad, P. V., Cook, B. D., Davis, K. J., and Carey, E. V.: Comparing net ecosystem exchange of carbon dioxide between an old-growth and mature forest in the upper Midwest, USA, *Agr. Forest Meteorol.*, 128, 33–55, doi:10.1016/j.agrformet.2004.09.005, 2005. 29187
- Dirmeyer, P. A.: The terrestrial segment of soil moisture–climate coupling, *Geophys. Res. Lett.*, 38, 1–5, doi:10.1029/2011GL048268, 2011. 29170
- Dirmeyer, P. A., Koster, R. D., and Guo, Z.: Do global models properly represent the feedback between land and atmosphere?, *J. Hydrometeorol.*, 7, 1177–1198, doi:10.1175/JHM532.1, 2006. 29142
- Ek, M. B. and Holtslag, A. A. M.: Influence of soil moisture on boundary layer cloud development, *J. Hydrometeorol.*, 5, 86–99, doi:10.1175/1525-7541(2004)005<0086:IOSMOB>2.0.CO;2, 2004. 29140, 29141
- Ek, M. B., Mitchell, K. E., Lin, Y., Rogers, E., Grunmann, P., Koren, V., Gayno, G., and Tarp-ley, J. D.: Implementation of Noah land surface model advances in the National Centers for Environmental Prediction operational mesoscale Eta model, *J. Geophys. Res.*, 108, 8851, doi:10.1029/2002JD003296, 2003. 29145
- Ferguson, C. R., Wood, E. F., and Vinukollu, R. K.: A global intercomparison of modeled and observed land–atmosphere coupling, *J. Hydrometeorol.*, 13, 749–784, doi:10.1175/JHM-D-11-0119.1, 2012. 29166, 29170
- Fernandez, I. J., Rustad, L. E., and Lawrence, G. B.: Estimating total soil mass, nutrient content, and trace metals in soils under a low elevation spruce-fir forest, *Can. J. Soil Sci.*, 73, 317–328, doi:10.4141/cjss93-034, 1993. 29186
- Findell, K. L., and Eltahir, E. A. B.: Atmospheric controls on soil moisture–boundary layer interactions, Part 1: Framework development, *J. Hydrometeorol.*, 4, 552–569, doi:10.1175/1525-7541(2003)004<0552:ACOSML>2.0.CO;2, 2003a. 29140, 29141, 29151, 29170
- Findell, K. L. and Eltahir, E. A. B.: Atmospheric controls on soil moisture–boundary layer interactions, Part 2: Feedbacks within the continental United States, *J. Hydrometeorol.*, 4, 570–583, doi:10.1175/1525-7541(2003)004<0570:ACOSML>2.0.CO;2, 2003b. 29140, 29141
- Findell, K. L., Gentine, P., Lintner, B. R., and Kerr, C.: Probability of afternoon precipitation in eastern United States and Mexico enhanced by high evaporation, *Nat. Geosci.*, 4, 434–439, doi:10.1038/ngeo1174, 2011. 29143, 29144, 29151, 29152, 29153, 29154, 29155, 29165, 29170

Land surface controls on afternoon precipitation

B. P. Guillod et al.

Title Page

Abstract

Introduction

Conclusions

References

Tables

Figures

◀

▶

◀

▶

Back

Close

Full Screen / Esc

Printer-friendly Version

Interactive Discussion



- Fischer, M. L., Billesbach, D. P., Berry, J. A., Riley, W. J., and Torn, M. S.: Spatiotemporal variations in growing season exchanges of CO₂, H₂O, and sensible heat in agricultural fields of the southern Great Plains, *Earth Interact.*, 11, 1–21, doi:10.1175/EI231.1, 2007. 29186
- 5 Fisher, J. B., Tu, K. P., and Baldocchi, D. D.: Global estimates of the land–atmosphere water flux based on monthly AVHRR and ISLSCP-II data, validated at 16 FLUXNET sites, *Remote Sens. Environ.*, 112, 901–919, doi:10.1016/j.rse.2007.06.025, 2008. 29186
- Foken, T.: The energy balance closure problem: an overview, *Ecol. Appl.*, 18, 1351–1367, doi:10.1890/06-0922.1, 2008. 29146
- 10 Gash, J. H. C.: An analytical model of rainfall interception by forests, *Q. J. Roy. Meteor. Soc.*, 105, 43–55, doi:10.1002/qj.49710544304, 1979. 29147
- Gentine, P., Polcher, J., and Entekhabi, D.: Harmonic propagation of variability in surface energy balance within a coupled soil-vegetation-atmosphere system, *Water Resour. Res.*, 47, 1–21, doi:10.1029/2010WR009268, 2011. 29143
- 15 Gentine, P., Holtlag, A. A. M., D’Andrea, F., and Ek, M.: Surface and atmospheric controls on the onset of moist convection over land, *J. Hydrometeorol.*, 14, 1443–1462, doi:10.1175/JHM-D-12-0137.1, 2013. 29140
- Gerrits, A. and Savenije, H.: 2.04 – Interception, in: *Treatise on Water Science*, edited by: Peter Wilderer, E., Elsevier, Oxford, 89–101, 2011. 29163, 29167
- 20 Gianotti, D., Anderson, B. T., and Salvucci, G. D.: What do rain gauges tell us about the limits of precipitation predictability?*, *J. Climate*, 26, 5682–5688, doi:10.1175/JCLI-D-12-00718.1, 2013. 29166
- Goldstein, A., Hultman, N., Fracheboud, J., Bauer, M., Panek, J., Xu, M., Qi, Y., Guenther, A., and Baugh, W.: Effects of climate variability on the carbon dioxide, water, and sensible heat fluxes above a ponderosa pine plantation in the Sierra Nevada (CA), *Agr. Forest Meteorol.*, 25 101, 113–129, doi:10.1016/S0168-1923(99)00168-9, 2000. 29186
- Greco, S. and Baldocchi, D. D.: Seasonal variations of CO₂ and water vapour exchange rates over a temperate deciduous forest, *Glob. Change Biol.*, 2, 183–197, doi:10.1111/j.1365-2486.1996.tb00071.x, 1996. 29187
- 30 Gu, L., Meyers, T., Pallardy, S. G., Hanson, P. J., Yang, B., Heuer, M., Hosman, K. P., Liu, Q., Riggs, J. S., Sluss, D., and Wullschleger, S. D.: Influences of biomass heat and biochemical energy storages on the land surface fluxes and radiative temperature, *J. Geophys. Res.*, 112, D02107, doi:10.1029/2006JD007425, 2007. 29186

Land surface controls on afternoon precipitation

B. P. Guillod et al.

Title Page

Abstract

Introduction

Conclusions

References

Tables

Figures

◀

▶

◀

▶

Back

Close

Full Screen / Esc

Printer-friendly Version

Interactive Discussion



Guillod, B., Davin, E., Kündig, C., Smiatek, G., and Seneviratne, S.: Impact of soil map specifications for European climate simulations, *Clim. Dynam.*, 40, 123–141, doi:10.1007/s00382-012-1395-z, 2013. 29158

Heinsch, F., Heilman, J., McInnes, K., Cobos, D., Zuberer, D., and Roelke, D.: Carbon dioxide exchange in a high marsh on the Texas Gulf Coast: effects of freshwater availability, *Agr. Forest Meteorol.*, 125, 159–172, 2004. 29186

Hendricks Franssen, H., Stöckli, R., Lehner, I., Rotenberg, E., and Seneviratne, S.: Energy balance closure of eddy-covariance data: a multisite analysis for European FLUXNET stations, *Agr. Forest Meteorol.*, 150, 1553–1567, doi:10.1016/j.agrformet.2010.08.005, 2010. 29146

Hirschi, M., Seneviratne, S. I., Alexandrov, V., Boberg, F., Boroneant, C., Christensen, O. B., Formayer, H., Orlowsky, B., and Stepanek, P.: Observational evidence for soil-moisture impact on hot extremes in southeastern Europe, *Nat. Geosci.*, 4, 17–21, doi:10.1038/ngeo1032, 2011. 29141

Hohenegger, C., Brockhaus, P., Bretherton, C. S., and Schär, C.: The soil moisture–precipitation feedback in simulations with explicit and parameterized convection, *J. Climate*, 22, 5003–5020, doi:10.1175/2009JCLI2604.1, 2009. 29140, 29141

Holwerda, F., Bruijnzeel, L., Scatena, F., Vugts, H., and Meesters, A.: Wet canopy evaporation from a Puerto Rican lower montane rain forest: the importance of realistically estimated aerodynamic conductance, *J. Hydrol.*, 414–415, 1–15, 2012. 29149

Hsu, K.-I., Gao, X., Sorooshian, S., and Gupta, H. V.: Precipitation estimation from remotely sensed information using artificial neural networks, *J. Appl. Meteorol.*, 36, 1176–1190, doi:10.1175/1520-0450(1997)036<1176:PEFRSI>2.0.CO;2, 1997. 29150

Huffman, G. J., Adler, R. F., Morrissey, M. M., Bolvin, D. T., Curtis, S., Joyce, R., McGavock, B., and Susskind, J.: Global precipitation at one-degree daily resolution from multisatellite observations, *J. Hydrometeorol.*, 2, 36–50, doi:10.1175/1525-7541(2001)002<0036:GPAODD>2.0.CO;2, 2001. 29149

Johnson, D. W.: Simulated nitrogen cycling response to elevated CO₂ in *Pinus taeda* and mixed deciduous forests, *Tree Physiol.*, 19, 321–327, 1999. 29186

Katul, G., Leuning, R., and Oren, R.: Relationship between plant hydraulic and biochemical properties derived from a steady-state coupled water and carbon transport model, *Plant Cell Environ.*, 26, 339–350, doi:10.1046/j.1365-3040.2003.00965.x, 2003. 29186

**Land surface
controls on afternoon
precipitation**B. P. Guillod et al.

Title Page

Abstract

Introduction

Conclusions

References

Tables

Figures

◀

▶

◀

▶

Back

Close

Full Screen / Esc

Printer-friendly Version

Interactive Discussion



- Kennedy, A. D., Dong, X., Xi, B., Xie, S., Zhang, Y., and Chen, J.: A comparison of MERRA and NARR reanalyses with the DOE ARM SGP data, *J. Climate*, 24, 4541–4557, doi:10.1175/2011JCLI3978.1, 2011. 29144
- Koster, R. D. and Suarez, M. J.: Soil moisture memory in climate models, *J. Hydrometeorol.*, 2, 558–570, doi:10.1175/1525-7541(2001)002<0558:SMMICM>2.0.CO;2, 2001. 29162
- Koster, R. D., Suarez, M. J., Higgins, R. W., and Van den Dool, H. M.: Observational evidence that soil moisture variations affect precipitation, *Geophys. Res. Lett.*, 30, 1–4, doi:10.1029/2002GL016571, 2003. 29142
- Koster, R. D., Dirmeyer, P. A., Guo, Z., Bonan, G., Chan, E., Cox, P., Gordon, C. T., Kanae, S., Kowalczyk, E., Lawrence, D., Liu, P., Lu, C.-H., Malyshev, S., McAvaney, B., Mitchell, K., Mocko, D., Oki, T., Oleson, K., Pitman, A., Sud, Y. C., Taylor, C. M., Verseghy, D., Vasic, R., Xue, Y., and Yamada, T.: Regions of strong coupling between soil moisture and precipitation, *Science*, 305, 1138–1140, doi:10.1126/science.1100217, 2004. 29141, 29155, 29166, 29168, 29169
- Koster, R. D., Mahanama, S. P. P., Yamada, T. J., Balsamo, G., Berg, A. A., Boissarie, M., Dirmeyer, P. A., Doblas-Reyes, F. J., Drewitt, G., Gordon, C. T., Guo, Z., Jeong, J.-H., Lawrence, D. M., Lee, W.-S., Li, Z., Luo, L., Malyshev, S., Merryfield, W. J., Seneviratne, S. I., Stanelle, T., van den Hurk, B. J. J. M., Vitart, F., and Wood, E. F.: Contribution of land surface initialization to subseasonal forecast skill: first results from a multi-model experiment, *Geophys. Res. Lett.*, 37, 1–6, doi:10.1029/2009GL041677, 2010. 29162
- Langley, J., Drake, B., and Hungate, B.: Extensive belowground carbon storage supports roots and mycorrhizae in regenerating scrub oaks, *Oecologia*, 131, 542–548, doi:10.1007/s00442-002-0932-6, 2002. 29186
- Lintner, B. R., Gentine, P., Findell, K. L., D’Andrea, F., Sobel, A. H., and Salvucci, G. D.: An idealized prototype for large-scale land–atmosphere coupling, *J. Climate*, 26, 2379–2389, doi:10.1175/JCLI-D-11-00561.1, 2013. 29140
- Ma, S., Baldocchi, D. D., Xu, L., and Hehn, T.: Inter-annual variability in carbon dioxide exchange of an oak/grass savanna and open grassland in California, *Agr. Forest Meteorol.*, 147, 157–171, doi:10.1016/j.agrformet.2007.07.008, 2007. 29187
- Mackay, D. S., Ahl, D. E., Ewers, B. E., Gower, S. T., Burrows, S. N., Samanta, S., and Davis, K. J.: Effects of aggregated classifications of forest composition on estimates of evapotranspiration in a northern Wisconsin forest, *Glob. Change Biol.*, 8, 1253–1265, doi:10.1046/j.1365-2486.2002.00554.x, 2002. 29187

Land surface controls on afternoon precipitation

B. P. Guillod et al.

Title Page

Abstract

Introduction

Conclusions

References

Tables

Figures

◀

▶

◀

▶

Back

Close

Full Screen / Esc

Printer-friendly Version

Interactive Discussion



Mahfouf, J.-F.: Analysis of soil moisture from near-surface parameters: a feasibility study, *J. Appl. Meteorol.*, 30, 1534–1547, doi:10.1175/1520-0450(1991)030<1534:AOSMFN>2.0.CO;2, 1991. 29143

Matamala, R., Jastrow, J. D., Miller, R. M., and Garten, C. T.: Temporal changes in C and N stocks of restored prairie: implications for C sequestration strategies, *Ecol. Appl.*, 18, 1470–1488, doi:10.1890/07-1609.1, 2008. 29186

McLaren, J. D., Arain, M. A., Khomik, M., Peichl, M., and Brodeur, J.: Water flux components and soil water-atmospheric controls in a temperate pine forest growing in a well-drained sandy soil, *J. Geophys. Res.*, 113, G04031, doi:10.1029/2007JG000653, 2008. 29167

Mesinger, F., DiMego, G., Kalnay, E., Mitchell, K., Shafran, P. C., Ebisuzaki, W., Jović, D., Woollen, J., Rogers, E., Berbery, E. H., Ek, M. B., Fan, Y., Grumbine, R., Higgins, W., Li, H., Lin, Y., Manikin, G., Parrish, D., and Shi, W.: North American regional reanalysis, *B. Am. Meteorol. Soc.*, 87, 343–360, doi:10.1175/BAMS-87-3-343, 2006. 29144

Miralles, D. G., Gash, J. H., Holmes, T. R. H., de Jeu, R. A. M., and Dolman, A. J.: Global canopy interception from satellite observations, *J. Geophys. Res.*, 115, D16122, doi:10.1029/2009JD013530, 2010. 29147

Miralles, D. G., De Jeu, R. A. M., Gash, J. H., Holmes, T. R. H., and Dolman, A. J.: Magnitude and variability of land evaporation and its components at the global scale, *Hydrol. Earth Syst. Sci.*, 15, 967–981, doi:10.5194/hess-15-967-2011, 2011a. 29167

Miralles, D. G., Holmes, T. R. H., De Jeu, R. A. M., Gash, J. H., Meesters, A. G. C. A., and Dolman, A. J.: Global land-surface evaporation estimated from satellite-based observations, *Hydrol. Earth Syst. Sci.*, 15, 453–469, doi:10.5194/hess-15-453-2011, 2011b. 29147, 29148, 29149, 29170

Mizutani, K., Yamanoi, K., Ikeda, T., and Watanabe, T.: Applicability of the eddy correlation method to measure sensible heat transfer to forest under rainfall conditions, *Agr. Forest Meteorol.*, 86, 193–203, doi:10.1016/S0168-1923(97)00012-9, 1997. 29167

Monson, R. K., Turnipseed, A. A., Sparks, J. P., Harley, P. C., Scott-Denton, L. E., Sparks, K., and Huxman, T. E.: Carbon sequestration in a high-elevation, subalpine forest, *Glob. Change Biol.*, 8, 459–478, doi:10.1046/j.1365-2486.2002.00480.x, 2002. 29186

Mueller, B. and Seneviratne, S. I.: Hot days induced by precipitation deficits at the global scale, *P. Natl. Acad. Sci. USA*, 109, 12398–12403, doi:10.1073/pnas.1204330109, 2012. 29168

Land surface controls on afternoon precipitation

B. P. Guillod et al.

Title Page

Abstract

Introduction

Conclusions

References

Tables

Figures

◀

▶

◀

▶

Back

Close

Full Screen / Esc

Printer-friendly Version

Interactive Discussion

- Noormets, A., Chen, J., and Crow, T.: Age-dependent changes in ecosystem carbon fluxes in managed forests in Northern Wisconsin, USA, *Ecosystems*, 10, 187–203, doi:10.1007/s10021-007-9018-y, 2007. 29187
- Orlowsky, B. and Seneviratne, S. I.: Statistical analyses of land–atmosphere feedbacks and their possible pitfalls, *J. Climate*, 23, 3918–3932, doi:10.1175/2010JCLI3366.1, 2010. 29142
- Owe, M., de Jeu, R., and Holmes, T.: Multisensor historical climatology of satellite-derived global land surface moisture, *J. Geophys. Res.*, 113, F01002, doi:10.1029/2007JF000769, 2008. 29148, 29188
- Owen, K. E., Tenhunen, J., Reichstein, M., Wang, Q., Falge, E., Geyer, R., Xiao, X., Stoy, P., Ammann, C., Arain, A., Aubinet, M., Aurela, M., Bernhofer, C., Chojnicki, B. H., Granier, A., Gruenwald, T., Hadley, J., Heinesch, B., Hollinger, D., Knohl, A., Kutsch, W., Lohila, A., Meyers, T., Moors, E., Moureaux, C., Pilegaard, K., Saigusa, N., Verma, S., Vesala, T., and Vogel, C.: Linking flux network measurements to continental scale simulations: ecosystem carbon dioxide exchange capacity under non-water-stressed conditions, *Glob. Change Biol.*, 13, 734–760, doi:10.1111/j.1365-2486.2007.01326.x, 2007. 29186
- Pal, J. S. and Eltahir, E. A. B.: Pathways relating soil moisture conditions to future summer rainfall within a model of the land–atmosphere system, *J. Climate*, 14, 1227–1242, doi:10.1175/1520-0442(2001)014<1227:PRSMCT>2.0.CO;2, 2001. 29140, 29141
- Priestley, C. H. B. and Taylor, R. J.: On the assessment of surface heat flux and evaporation using large-scale parameters, *Mon. Weather Rev.*, 100, 81–92, doi:10.1175/1520-0493(1972)100<0081:OTAOSH>2.3.CO;2, 1972. 29147
- Pryor, S. C., Barthelmie, R. J., and Jensen, B.: Nitrogen dry deposition at an AmeriFlux site in a hardwood forest in the midwest, *Geophys. Res. Lett.*, 26, 691–694, doi:10.1029/1999GL900066, 1999. 29186
- Rio, C., Hourdin, F., Grandpeix, J.-Y., and Lafore, J.-P.: Shifting the diurnal cycle of parameterized deep convection over land, *Geophys. Res. Lett.*, 36, L07809, doi:10.1029/2008GL036779, 2009. 29152
- Roulet, N. T., Lafleur, P. M., Richard, P. J. H., Moore, T. R., Humphreys, E. R., and Bubier, J.: Contemporary carbon balance and late Holocene carbon accumulation in a northern peatland, *Glob. Change Biol.*, 13, 397–411, doi:10.1111/j.1365-2486.2006.01292.x, 2007. 29186
- Ruane, A. C.: NARR's atmospheric water cycle components, Part 1: 20-year mean and annual interactions, *J. Hydrometeorol.*, 11, 1205–1219, doi:10.1175/2010JHM1193.1, 2010a. 29144

**Land surface
controls on afternoon
precipitation**

B. P. Guillod et al.

Title Page

Abstract

Introduction

Conclusions

References

Tables

Figures

◀

▶

◀

▶

Back

Close

Full Screen / Esc

Printer-friendly Version

Interactive Discussion



Ruane, A. C.: NARR's atmospheric water cycle components, Part 2: Summertime mean and diurnal interactions, *J. Hydrometeorol.*, 11, 1220–1233, doi:10.1175/2010JHM1279.1, 2010b. 29144

Saito, M., Maksyutov, S., Hirata, R., and Richardson, A. D.: An empirical model simulating diurnal and seasonal CO₂ flux for diverse vegetation types and climate conditions, *Biogeosciences*, 6, 585–599, doi:10.5194/bg-6-585-2009, 2009. 29186

Salvucci, G. D. and Entekhabi, D.: Equivalent steady soil moisture profile and the time compression approximation in water balance modeling, *Water Resour. Res.*, 30, 2737–2749, doi:10.1029/94WR00948, 1994. 29162

Salvucci, G. D., Saleem, J. A., and Kaufmann, R.: Investigating soil moisture feedbacks on precipitation with tests of Granger causality, *Adv. Water Resour.*, 25, 1305–1312, doi:10.1016/S0309-1708(02)00057-X, 2002. 29142, 29160

Santanello, J. A., Peters-Lidard, C. D., Kumar, S. V., Alonge, C., and Tao, W.-K.: A modeling and observational framework for diagnosing local land–atmosphere coupling on diurnal time scales, *J. Hydrometeorol.*, 10, 577–599, doi:10.1175/2009JHM1066.1, 2009. 29140

Savenije, H.: Does moisture feedback affect rainfall significantly?, *Phys. Chem. Earth*, 20, 507–513, doi:10.1016/S0079-1946(96)00014-6, 1995a. 29170

Savenije, H. H.: New definitions for moisture recycling and the relationship with land-use changes in the Sahel, *J. Hydrol.*, 167, 57–78, doi:10.1016/0022-1694(94)02632-L, 1995b. 29163, 29170

Savenije, H. H. G.: The importance of interception and why we should delete the term evapotranspiration from our vocabulary, *Hydrol. Process.*, 18, 1507–1511, doi:10.1002/hyp.5563, 2004. 29163, 29167

Schär, C., Lüthi, D., Beyerle, U., and Heise, E.: The soil–precipitation feedback: a process study with a regional climate model, *J. Climate*, 12, 722–741, doi:10.1175/1520-0442(1999)012<0722:TSPFAP>2.0.CO;2, 1999. 29140, 29141

Schmid, H.: Source areas for scalars and scalar fluxes, *Bound.-Lay. Meteorol.*, 67, 293–318, doi:10.1007/BF00713146, 1994. 29158

Schwalm, C. R., Williams, C. A., Schaefer, K., Baldocchi, D., Black, T. A., Goldstein, A. H., Law, B. E., Oechel, W. C., Paw U, K. T., and Scott, R. L.: Reduction in carbon uptake during turn of the century drought in western North America, *Nat. Geosci.*, 5, 551–556, doi:10.1038/ngeo1529, 2012. 29155, 29169

Land surface controls on afternoon precipitation

B. P. Guillod et al.

Title Page

Abstract

Introduction

Conclusions

References

Tables

Figures

◀

▶

◀

▶

Back

Close

Full Screen / Esc

Printer-friendly Version

Interactive Discussion



Scott, R., Koster, R. D., Entekhabi, D., and Suarez, M. J.: Effect of a canopy interception reservoir on hydrological persistence in a general circulation model, *J. Climate*, 8, 1917–1922, doi:10.1175/1520-0442(1995)008<1917:EOACIR>2.0.CO;2, 1995. 29163

5 Scott, R., Entekhabi, D., Koster, R., and Suarez, M.: Timescales of land surface evapotranspiration response, *J. Climate*, 10, 559–566, doi:10.1175/1520-0442(1997)010<0559:TOLSER>2.0.CO;2, 1997. 29162, 29163

Scott, R. L., Jenerette, G. D., Potts, D. L., and Huxman, T. E.: Effects of seasonal drought on net carbon dioxide exchange from a woody-plant-encroached semiarid grassland, *J. Geophys. Res.*, 114, G04004, doi:10.1029/2008JG000900, 2009. 29187

10 Scott, R. L., Hamerlynck, E. P., Jenerette, G. D., Moran, M. S., and Barron-Gafford, G. A.: Carbon dioxide exchange in a semidesert grassland through drought-induced vegetation change, *J. Geophys. Res.*, 115, G03026, doi:10.1029/2010JG001348, 2010. 29187

Seneviratne, S. I., Viterbo, P., Lüthi, D., and Schär, C.: Inferring changes in terrestrial water storage using ERA-40 reanalysis data: the Mississippi River Basin, *J. Climate*, 17, 2039–2057, doi:10.1175/1520-0442(2004)017<2039:ICITWS>2.0.CO;2, 2004. 29143

15 Seneviratne, S. I., Koster, R. D., Guo, Z., Dirmeyer, P. A., Kowalczyk, E., Lawrence, D., Liu, P., Mocko, D., Lu, C.-H., Oleson, K. W., and Verseghy, D.: Soil moisture memory in AGCM simulations: analysis of Global Land–Atmosphere Coupling Experiment (GLACE) data, *J. Hydrometeorol.*, 7, 1090–1112, doi:10.1175/JHM533.1, 2006a. 29162

20 Seneviratne, S. I., Lüthi, D., Litschi, M., and Schär, C.: Land–atmosphere coupling and climate change in Europe, *Nature*, 443, 205–209, doi:10.1038/nature05095, 2006b. 29141

Seneviratne, S. I., Corti, T., Davin, E. L., Hirschi, M., Jaeger, E. B., Lehner, I., Orlowsky, B., and Teuling, A. J.: Investigating soil moisture–climate interactions in a changing climate: a review, *Earth-Sci. Rev.*, 99, 125–161, doi:10.1016/j.earscirev.2010.02.004, 2010. 29140, 29141, 29142, 29168, 29170, 29189

25 Sheffield, J., Goteti, G., and Wood, E. F.: Development of a 50-year high-resolution global dataset of meteorological forcings for land surface modeling, *J. Climate*, 19, 3088–3111, doi:10.1175/JCLI3790.1, 2006. 29188

Stackhouse, P. W., Gupta, S. K., Cox, S. J., Mikovitz, J. C., Zhang, T., and Chiacchio, M.: 12 year surface radiation budget data set, *GEWEX News*, 14, 10–12, 2004. 29148, 29188

30 Stöckli, R., Rutishauser, T., Baker, I., Liniger, M. A., and Denning, A. S.: A global reanalysis of vegetation phenology, *J. Geophys. Res.*, 116, G03020, doi:10.1029/2010JG001545, 2011. 29201

Land surface controls on afternoon precipitation

B. P. Guillod et al.

Title Page

Abstract

Introduction

Conclusions

References

Tables

Figures

◀

▶

◀

▶

Back

Close

Full Screen / Esc

Printer-friendly Version

Interactive Discussion



Stylinski, C., Gamon, J., and Oechel, W.: Seasonal patterns of reflectance indices, carotenoid pigments and photosynthesis of evergreen chaparral species, *Oecologia*, 131, 366–374, doi:10.1007/s00442-002-0905-9, 2002. 29187

Suyker, A., Verma, S., Burba, G., Arkebauer, T., Walters, D., and Hubbard, K.: Growing season carbon dioxide exchange in irrigated and rainfed maize, *Agr. Forest Meteorol.*, 124, 1–13, doi:10.1016/j.agrformet.2004.01.011, 2004. 29186

Taylor, C. M. and Ellis, R. J.: Satellite detection of soil moisture impacts on convection at the mesoscale, *Geophys. Res. Lett.*, 33, 11–14, doi:10.1029/2005GL025252, 2006. 29140

Taylor, C. M., Gounou, A., Guichard, F., Harris, P. P., Ellis, R. J., Couvreur, F., and De Kauwe, M.: Frequency of Sahelian storm initiation enhanced over mesoscale soil-moisture patterns, *Nat. Geosci.*, 4, 1–4, doi:10.1038/ngeo1173, 2011. 29140, 29170

Taylor, C. M., de Jeu, R. A. M., Guichard, F., Harris, P. P., and Dorigo, W. A.: Afternoon rain more likely over drier soils, *Nature*, 489, 423–426, doi:10.1038/nature11377, 2012. 29140, 29142, 29170

Teuling, A. J., Hirschi, M., Ohmura, A., Wild, M., Reichstein, M., Ciais, P., Buchmann, N., Ammann, C., Montagnani, L., Richardson, A. D., Wohlfahrt, G., and Seneviratne, S. I.: A regional perspective on trends in continental evaporation, *Geophys. Res. Lett.*, 36, 1–5, doi:10.1029/2008GL036584, 2009. 29141, 29168, 29201

Teuling, A. J., Seneviratne, S. I., Stöckli, R., Reichstein, M., Moors, E., Ciais, P., Luysaert, S., van den Hurk, B., Ammann, C., Bernhofer, C., Dellwik, E., Gianelle, D., Gielen, B., Grünwald, T., Klumpp, K., Montagnani, L., Moureaux, C., Sottocornola, M., and Wohlfahrt, G.: Contrasting response of European forest and grassland energy exchange to heatwaves, *Nat. Geosci.*, 3, 722–727, doi:10.1038/ngeo950, 2010. 29158, 29169

Thomas, C. K., Law, B. E., Irvine, J., Martin, J. G., Pettijohn, J. C., and Davis, K. J.: Seasonal hydrology explains interannual and seasonal variation in carbon and water exchange in a semiarid mature ponderosa pine forest in central Oregon, *J. Geophys. Res.*, 114, G04006, doi:10.1029/2009JG001010, 2009. 29155, 29186

Urbanski, S., Barford, C., Wofsy, S., Kucharik, C., Pyle, E., Budney, J., McKain, K., Fitzjarrald, D., Czikowsky, M., and Munger, J. W.: Factors controlling CO₂ exchange on timescales from hourly to decadal at Harvard Forest, *J. Geophys. Res.*, 112, G02020, doi:10.1029/2006JG000293, 2007. 29186

Land surface controls on afternoon precipitation

B. P. Guillod et al.

Title Page

Abstract

Introduction

Conclusions

References

Tables

Figures

◀

▶

◀

▶

Back

Close

Full Screen / Esc

Printer-friendly Version

Interactive Discussion



- van den Hurk, B. J. J. M. and van Meijgaard, E.: Diagnosing land–atmosphere interaction from a regional climate model simulation over West Africa, *J. Hydrometeorol.*, 11, 467–481, doi:10.1175/2009JHM1173.1, 2010. 29141
- Vickers, D., Thomas, C. K., Pettijohn, C., Martin, J. G., and Law, B. E.: Five years of carbon fluxes and inherent water-use efficiency at two semi-arid pine forests with different disturbance histories, *Tellus B*, 64, 17159, doi:10.3402/tellusb.v64i0.17159, 2012. 29169
- von Storch, H. and Zwiers, F.: *Statistical Analysis in Climate Research*, Cambridge University Press, Cambridge, UK, 1999. 29158, 29194
- Waring, R. H. and McDowell, N.: Use of a physiological process model with forestry yield tables to set limits on annual carbon balances, *Tree Physiol.*, 22, 179–188, doi:10.1093/treephys/22.2-3.179, 2002. 29187
- Wei, J. and Dirmeyer, P. A.: Toward understanding the large-scale land-atmosphere coupling in the models: roles of different processes, *Geophys. Res. Lett.*, 37, 1–5, doi:10.1029/2010GL044769, 2010. 29170
- West, G. L., Steenburgh, W. J., and Cheng, W. Y. Y.: Spurious grid-scale precipitation in the North American regional reanalysis, *Mon. Weather Rev.*, 135, 2168–2184, doi:10.1175/MWR3375.1, 2007. 29144
- Westra, D., Steeneveld, G. J., and Holtslag, A. A. M.: Some observational evidence for dry soils supporting enhanced relative humidity at the convective boundary layer top, *J. Hydrometeorol.*, 13, 1347–1358, doi:10.1175/JHM-D-11-0136.1, 2012. 29140
- Wilson, K., Goldstein, A., Falge, E., Aubinet, M., Baldocchi, D., Berbigier, P., Bernhofer, C., Ceulemans, R., Dolman, H., Field, C., Grelle, A., Ibrom, A., Law, B., Kowalski, A., Meyers, T., Moncrieff, J., Monson, R., Oechel, W., Tenhunen, J., Valentini, R., and Verma, S.: Energy balance closure at FLUXNET sites, *Agr. Forest Meteorol.*, 113, 223–243, doi:10.1016/S0168-1923(02)00109-0, 2002. 29146
- Xiao, J., Zhuang, Q., Law, B. E., Chen, J., Baldocchi, D. D., Cook, D. R., Oren, R., Richardson, A. D., Wharton, S., Ma, S., Martin, T. A., Verma, S. B., Suyker, A. E., Scott, R. L., Monson, R. K., Litvak, M., Hollinger, D. Y., Sun, G., Davis, K. J., Bolstad, P. V., Burns, S. P., Curtis, P. S., Drake, B. G., Falk, M., Fischer, M. L., Foster, D. R., Gu, L., Hadley, J. L., Katul, G. G., Matamala, R., McNulty, S., Meyers, T. P., Munger, J. W., Noormets, A., Oechel, W. C., Kyaw Tha Paw, U., Schmid, H. P., Starr, G., Torn, M. S., and Wofsy, S. C.: A continuous measure of gross primary production for the conterminous United States derived from MODIS

and AmeriFlux data, Remote Sens. Environ., 114, 576–591, doi:10.1016/j.rse.2009.10.013, 2010. 29186

Yi, C., Li, R., Bakwin, P. S., Desai, A., Ricciuto, D. M., Burns, S. P., Turnipseed, A. A., Wofsy, S. C., Munger, J. W., Wilson, K., and Monson, R. K.: A nonparametric method for separating photosynthesis and respiration components in CO₂ flux measurements, Geophys. Res. Lett., 31, L17107, doi:10.1029/2004GL020490, 2004. 29186

Yuan, W., Liu, S., Zhou, G., Zhou, G., Tieszen, L. L., Baldocchi, D., Bernhofer, C., Gholz, H., Goldstein, A. H., Goulden, M. L., Hollinger, D. Y., Hu, Y., LAW, B. E., Stoy, P. C., Vesala, T., and Wofsy, S. C.: Deriving a light use efficiency model from eddy covariance flux data for predicting daily gross primary production across biomes, Agr. Forest Meteorol., 143, 189–207, doi:10.1016/j.agrformet.2006.12.001, 2007. 29186

Land surface controls on afternoon precipitation

B. P. Guillod et al.

Title Page

Abstract

Introduction

Conclusions

References

Tables

Figures

◀

▶

◀

▶

Back

Close

Full Screen / Esc

Printer-friendly Version

Interactive Discussion



Land surface controls on afternoon precipitation

B. P. Guillod et al.

Title Page

Abstract

Introduction

Conclusions

References

Tables

Figures



Back

Close

Full Screen / Esc

Printer-friendly Version

Interactive Discussion



Table 1. List and description of datasets for the two main variables analyzed, the Evaporative Fraction (EF) and precipitation. Datasets are described in Sect. 2.

Dataset	Description
For EF	
NARR	Reanalysis (no direct observational constrain for surface fluxes)
FLUXNET	Ground-based measurement stations (Table 2)
GLEAM	Satellite-based remote-sensing-derived product (Table 3)
For Precipitation	
NARR	Reanalysis (assimilation from rain gauges)
NEXRAD	Remote-sensing product, ground-based radar

Land surface controls on afternoon precipitation

B. P. Guillod et al.

Title Page

Abstract

Introduction

Conclusions

References

Tables

Figures

◀

▶

◀

▶

Back

Close

Full Screen / Esc

Printer-friendly Version

Interactive Discussion

Table 2. FLUXNET sites included in this study, with latitude, longitude, altitude, vegetation class (IGBP, International Geosphere Biosphere Programme), years available, years excluded from the analysis and reference publication. IGBP classes represented in this subset of sites are: croplands (CRO), closed shrublands (CSH), deciduous broadleaf forests (DBF), evergreen needleleaf forests (ENF), grasslands (GRA), mixed forests (MF), permanent wetlands (WET) and woody savannas (WSA). For a detailed description of the vegetation classes, see <http://www.fluxdata.org/DataInfo/default.aspx/>, accessed on 21 June 2013.

Site	Lat [° N]	Lon [° E]	Altitude [m]	IGBP class	Years available	Years excluded	Reference
CA-Mer	45.41	-75.52	70	WET	1998–2005	2000	Roulet et al. (2007)
US-ARM	36.61	-97.49	314	CRO	2003–2006	–	Fischer et al. (2007)
US-Aud	31.59	-110.51	1469	GRA	2002–2006	–	Xiao et al. (2010)
US-Bkg	44.35	-96.84	510	GRA	2004–2006	–	Saito et al. (2009)
US-Blo	38.90	-120.63	1315	ENF	1997–2006	1997	Goldstein et al. (2000)
US-Bo1	40.01	-88.29	219	CRO	1996–2007	1996, 2007	Fisher et al. (2008)
US-Dk1	35.97	-79.09	168	GRA	2001–2005	–	Katul et al. (2003)
US-Dk3	35.98	-79.09	163	ENF	2001–2005	–	Johnson (1999)
US-FPe	48.31	-105.10	634	GRA	2000–2006	2001	Owen et al. (2007)
US-FR2	29.95	-97.00	271.9	WSA	2004–2006	–	Heinsch et al. (2004)
US-Goo	34.25	-89.87	87	GRA	2002–2006	2005	Yuan et al. (2007)
US-Ha1	42.54	-72.17	340	DBF	1991–2006	1991–1994, 1997, 2000–2005	Urbanski et al. (2007)
US-Ho1	45.20	-68.74	60	ENF	1996–2004	–	Fernandez et al. (1993)
US-Ho2	45.21	-68.75	91	ENF	1999–2004	–	Fernandez et al. (1993)
US-IB1	41.86	-88.22	225	CRO	2005–2007	–	Matamala et al. (2008)
US-IB2	41.84	-88.24	225	GRA	2004–2007	2004	Matamala et al. (2008)
US-KS2	28.61	-80.67	3	CSH	2000–2006	2003	Langley et al. (2002)
US-Los	46.08	-89.98	480	CSH	2001–2005	–	Yi et al. (2004)
US-LPH	42.54	-72.18	360–395	DBF	2002–2005	2005	Angert et al. (2003)
US-Me2	44.45	-121.56	1253	ENF	2003–2005	–	Thomas et al. (2009)
US-MMS	39.32	-86.41	275	DBF	1999–2005	1999, 2000	Pryor et al. (1999)
US-MOz	38.74	-92.20	219.4	DBF	2004–2006	–	Gu et al. (2007)
US-Ne3	41.18	-96.44	363	CRO	2001–2005	2005	Suyker et al. (2004)
US-NR1	40.03	-105.55	3050	ENF	1999–2003	–	Monson et al. (2002)

Land surface controls on afternoon precipitation

B. P. Guillod et al.

Table 2. Continued.

Site	Lat [° N]	Lon [° E]	Altitude [m]	IGBP class	Years available	Years excluded	Reference
US-PFa	45.95	−90.27	470	MF	1996–2003	1996	Mackay et al. (2002)
US-SO2	33.37	−116.62	1394	CSH	1997–2006	1997, 1998	Stylinski et al. (2002)
US-SO3	33.38	−116.62	1429	CSH	1997–2006	1998–2000, 2002–2004	Stylinski et al. (2002)
US-SP2	29.76	−82.24	50	ENF	1998–2004	1998, 1999	Bracho et al. (2011)
US-SP3	29.75	−82.16	50	ENF	1999–2004	1999	Bracho et al. (2011)
US-SRM	31.82	−110.87	1120	WSA	2004–2006	–	Scott et al. (2009)
US-Syv	46.24	−89.35	540	MF	2002–2006	2004	Desai et al. (2005)
US-Ton	38.43	−120.97	177	WSA	2001–2006	–	Ma et al. (2007)
US-UMB	45.56	−84.71	234	DBF	1999–2003	1999, 2002	Curtis et al. (2002)
US-Var	38.41	−120.95	129	GRA	2001–2006	2003, 2004	Ma et al. (2007)
US-WBW	35.96	−84.29	283	DBF	1995–1999	–	Greco and Baldocchi (1996)
US-WCr	45.81	−90.08	520	DBF	1999–2006	1999, 2004	Cook et al. (2004)
US-Wi4	46.74	−91.17	TBD	ENF	2002–2005	2003	Noormets et al. (2007)
US-Wkg	31.74	−109.94	1531	GRA	2004–2006	–	Scott et al. (2010)
US-Wrc	45.82	−121.95	371	ENF	1998–2006	2000, 2003, 2005, 2006	Waring and McDowell (2002)

Title Page

Abstract

Introduction

Conclusions

References

Tables

Figures

◀

▶

◀

▶

Back

Close

Full Screen / Esc

Printer-friendly Version

Interactive Discussion



Land surface controls on afternoon precipitation

B. P. Guillod et al.

Table 3. Datasets used in GLEAM product. Daily aggregates are computed locally to match the Evaporative Fraction (EF) estimate (i.e., starting and ending at around 9 a.m., see Sect. 2.4). S and E^{pot} are the evaporative stress and the potential evaporation, respectively. See Sect. 2.4 for details.

Variables	Dataset	Resolution and use
Soil moisture	NASA-LPRM (Owe et al., 2008)	night-time overpass (for the S calculation)
Vegetation optical depth	NASA-LPRM (Owe et al., 2008)	daily (for the S calculation)
Precipitation	NEXRAD (Sect. 2.3)	daily (for the S calculation)
Net radiation	GEWEX SRB 3.0 (Stackhouse et al., 2004)	daily (for the S calculations) and 3 hourly frequencies (for the morning E^{pot})
Air temperature	NCEP-1 (Sheffield et al., 2006)	daily (for the S calculations) and 3 hourly frequencies (for the morning E^{pot})

Title Page

Abstract

Introduction

Conclusions

References

Tables

Figures

◀

▶

◀

▶

Back

Close

Full Screen / Esc

Printer-friendly Version

Interactive Discussion



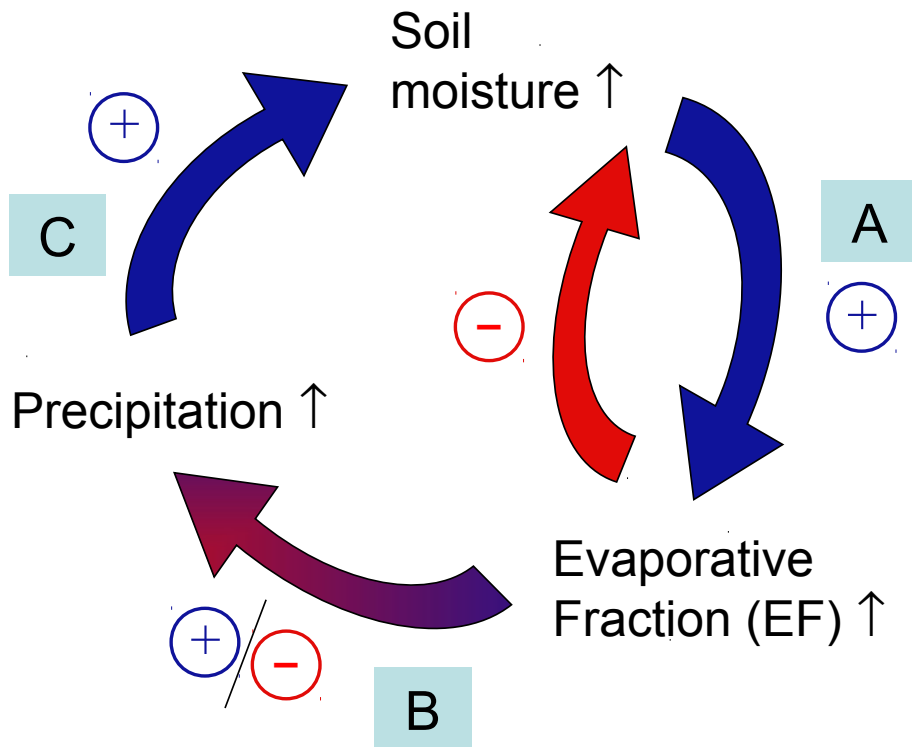


Fig. 1. Schematic description of soil moisture–precipitation coupling and feedback loop. Positive arrows (blue) indicate processes leading to a positive soil moisture–precipitation feedback (wetting for positive soil moisture anomaly, drying for negative soil moisture anomaly), the negative arrow (red) indicates a potential negative feedback damping the original soil moisture anomaly, and the red-blue arrow indicates the existence of both positive and negative feedbacks between evaporative fraction (EF) and precipitation anomalies. (A), (B) and (C) refer to the different steps of the feedback loop (see text). Modified from Seneviratne et al. (2010).

Title Page

Abstract

Introduction

Conclusions

References

Tables

Figures

◀

▶

◀

▶

Back

Close

Full Screen / Esc

Printer-friendly Version

Interactive Discussion



Land surface controls on afternoon precipitation

B. P. Guillod et al.

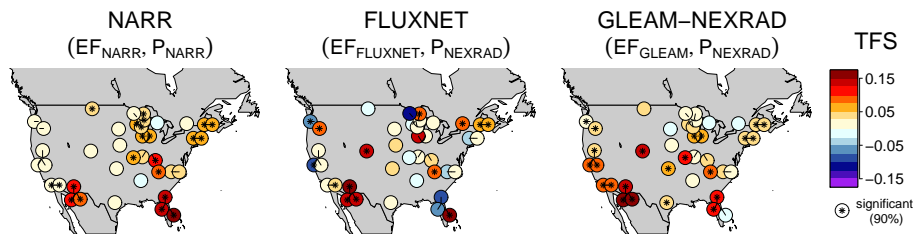


Fig. 2. Triggering Feedback Strength (TFS*) in different datasets computed at Fluxnet sites. (left) Evaporative Fraction (EF) and precipitation data from NARR, (center) EF from FLUXNET and precipitation from NEXRAD, and (right) EF from GLEAM and precipitation from NEXRAD. TFS* values significantly different from 0 at the 90 % level are indicated by a black star. In case of overlap, points are shifted and the black lines inside the circles indicate the actual location of the station.

Title Page

Abstract

Introduction

Conclusions

References

Tables

Figures

◀

▶

◀

▶

Back

Close

Full Screen / Esc

Printer-friendly Version

Interactive Discussion



Land surface controls on afternoon precipitation

B. P. Guillod et al.

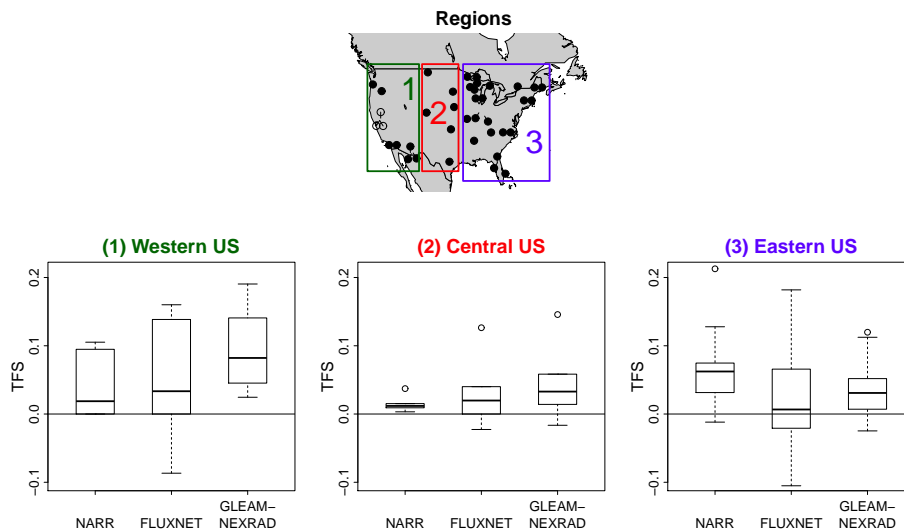


Fig. 3. Quantitative comparison of the Triggering Feedback Strength (TFS^*) in different regions for the three datasets shown in Fig. 2. (top) definition of the regions. (bottom) boxplot of TFS^* in the three regions (from left to right: Western, Central and Eastern US). Empty dots on the map indicate stations where results from GLEAM and NEXRAD should be interpreted with caution due to issues in NEXRAD data.

[Title Page](#)
[Abstract](#)
[Introduction](#)
[Conclusions](#)
[References](#)
[Tables](#)
[Figures](#)
[◀](#)
[▶](#)
[◀](#)
[▶](#)
[Back](#)
[Close](#)
[Full Screen / Esc](#)
[Printer-friendly Version](#)
[Interactive Discussion](#)

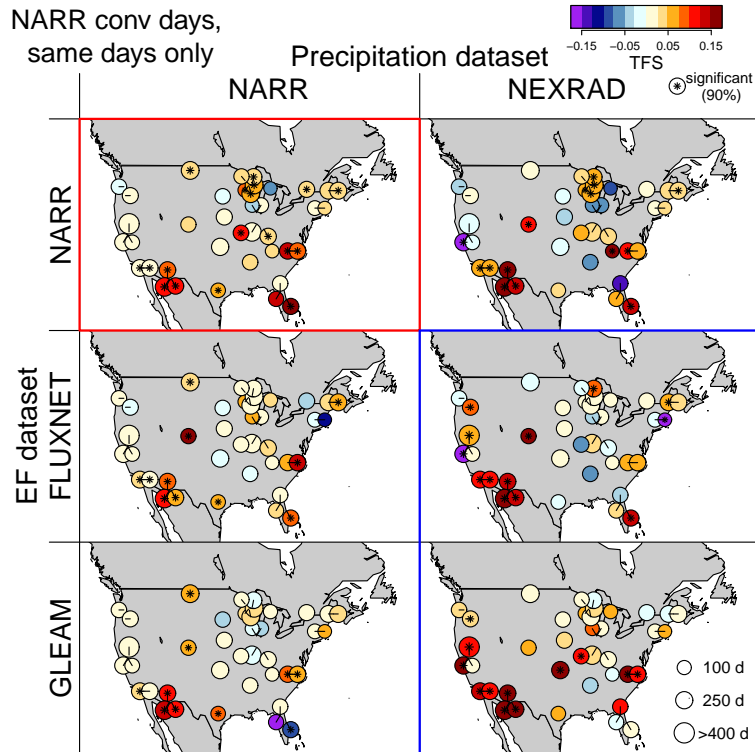



Fig. 4. Influence of dataset and sample size on TFS*. Only days with data in all datasets are included in the computation, and potentially convective days are further selected based on NARR (see Sect. 3.2 for the criteria). TFS* from NARR is boxed in red; TFS* from observation-based combinations in blue. TFS* values significantly different from 0 at the 90 % level are indicated by a black star.

Land surface controls on afternoon precipitation

B. P. Guillod et al.

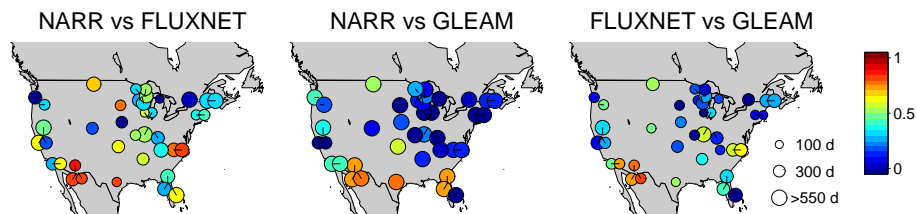


Fig. 5. Correlation of JJA before-noon EF values between different datasets. The size of the dots indicates the number of days included in the computation according to the legend shown on the bottom right.

[Title Page](#)[Abstract](#)[Introduction](#)[Conclusions](#)[References](#)[Tables](#)[Figures](#)[◀](#)[▶](#)[◀](#)[▶](#)[Back](#)[Close](#)[Full Screen / Esc](#)[Printer-friendly Version](#)[Interactive Discussion](#)

Land surface controls on afternoon precipitation

B. P. Guillod et al.

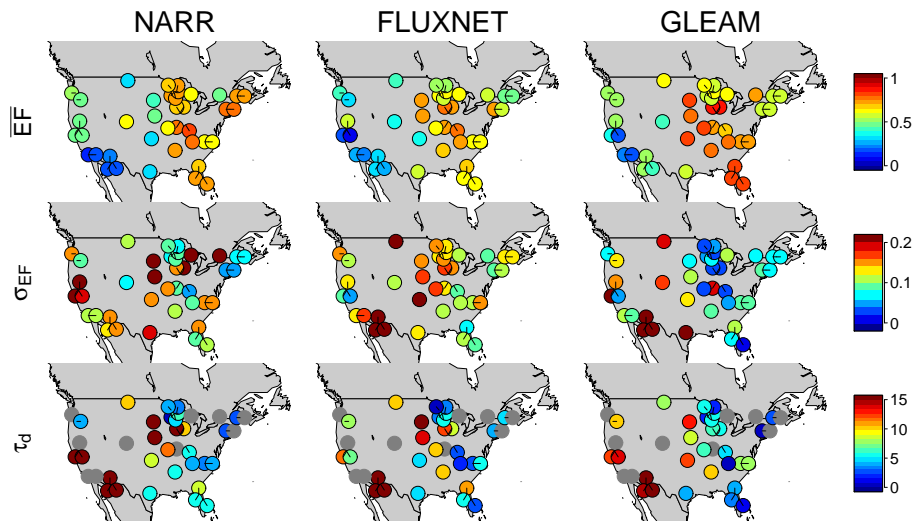


Fig. 6. Properties of EF datasets (NARR, FLUXNET, GLEAM, from left to right): (top) mean (\overline{EF}), (middle) standard deviation (σ_{EF}), (bottom) decorrelation time scale (τ_d). Only days with data in all three datasets are included in the computation to allow for a fair comparison. The decorrelation time scale τ_d is computed following von Storch and Zwiers (1999). Grey dots indicate too many gaps for a reliable quantification of τ_d .

Title Page

Abstract

Introduction

Conclusions

References

Tables

Figures

◀

▶

◀

▶

Back

Close

Full Screen / Esc

Printer-friendly Version

Interactive Discussion



Land surface controls on afternoon precipitation

B. P. Guillod et al.

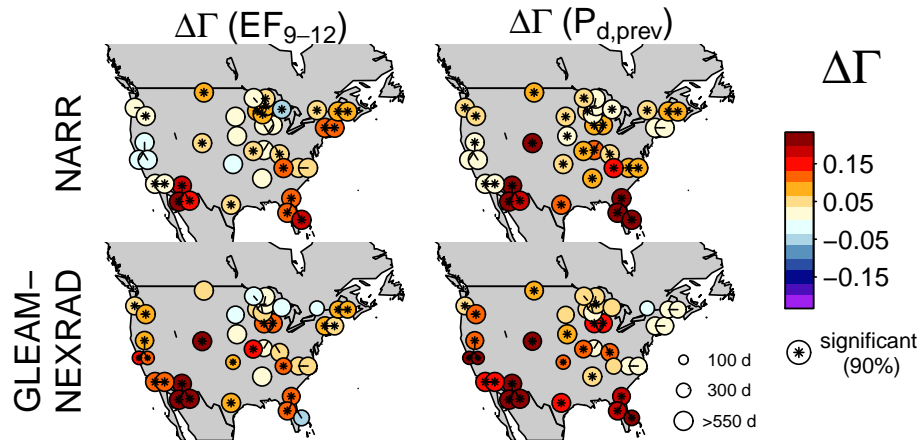


Fig. 7. Difference in the probability of afternoon rainfall ($\Delta\Gamma$) on days with high vs. low X where X is the before-noon EF (left panels) or previous day precipitation (right panels), for NARR (top row) and GLEAM-NEXRAD (bottom row). High (low) X refer to values higher (lower) than the 60th (40th) percentile of X , i.e. $\Delta\Gamma(X) = \Gamma(r|X > X_{Q60}) - \Gamma(r|X \leq X_{Q40})$. Values significantly different from 0 at the 90 % level are indicated by a black star. The size of the dots indicates the number of days included in the computation according to the legend shown on the bottom right map.

Land surface controls on afternoon precipitation

B. P. Guillod et al.

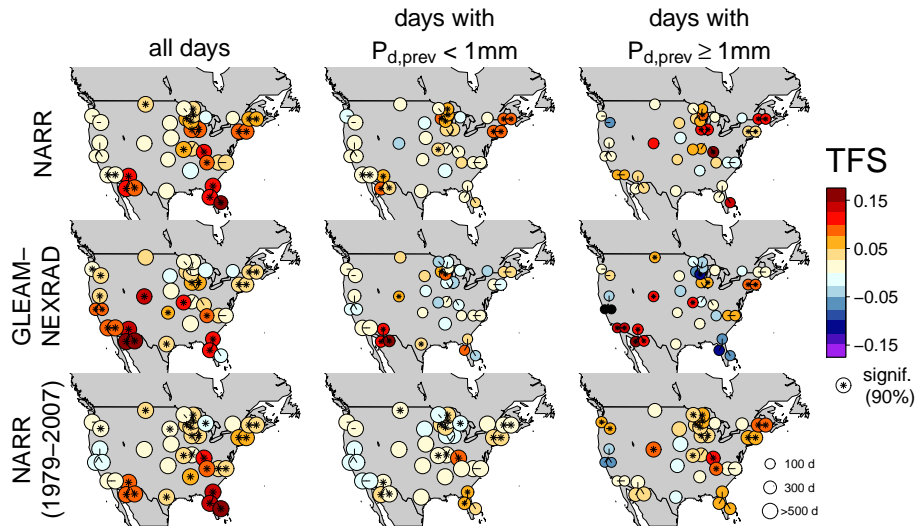


Fig. 8. TFS* for subset of days: (left) all days, (center) days without and (right) days with rainfall on the previous day, to account for precipitation persistence. Top row: NARR (years 1995–2007, as in the rest of the analysis). Middle row: GLEAM-NEXRAD combination. Bottom row: NARR, all years (1979–2007) for comparison, as the conditioning on previous day precipitation reduces the number of days available for the computation. The size of the dots indicates the number of days included in the computation according to the legend shown on the bottom right map.

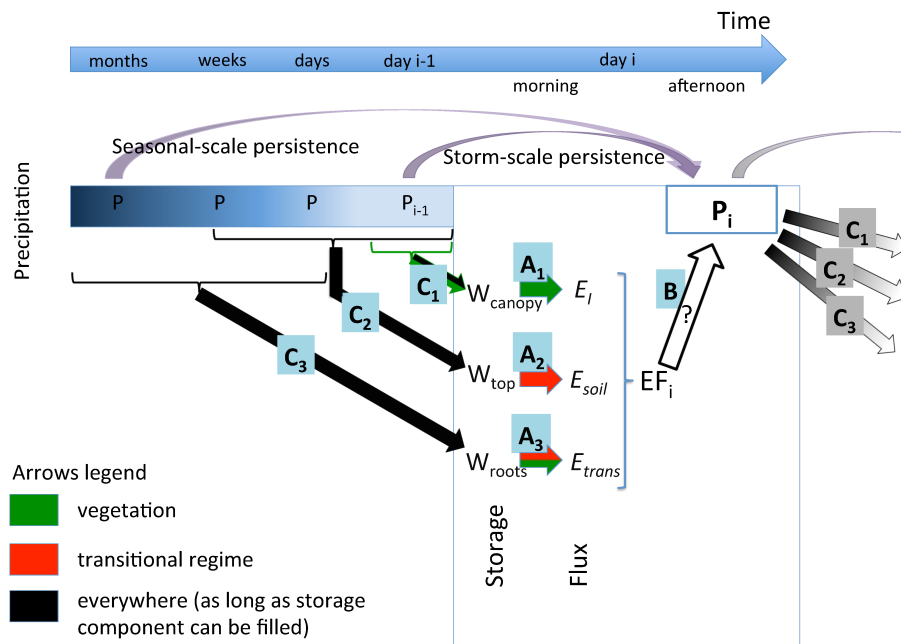


Fig. 9. Caption on next page.

Land surface controls on afternoon precipitation

B. P. Guillod et al.

Fig. 9. Schematic representation of soil moisture-precipitation feedback with individual components of land evaporation. The letters (A_i , B_i , C_i) refer to the steps of the feedback loop shown in Fig. 1, where “ i ” indicates the evaporation component concerned (1 for evaporation from vegetation interception, E_i ; 2 for bare soil evaporation, E_{soil} ; 3 for plant transpiration, E_{trans}). The horizontal axis represents time, ending on day i , and precipitation over the past days to months is represented as well as its typical influence on the three water storage term: canopy or vegetation interception storage W_{canopy} , impacted by previous day precipitation only (C_1); surface soil moisture W_{top} , impacted by precipitation in the previous days to weeks (C_2); and root zone soil moisture W_{root} , mainly impacted by precipitation in the previous weeks to months (C_3). These three storage terms then mainly impact their respective evaporation components, and thus EF, in different regions: over vegetated areas for interception (A_1), in a transitional soil moisture-climate regime for soil evaporation (A_2), and in regions which are both vegetated and in a transitional climate regime for transpiration (A_3). Note that A_2 and A_3 can also occur in other regions in some circumstances (e.g. over wet regions, during dry years). W_{root} includes W_{top} . Precipitation persistence at a sub-seasonal scale and storm-scale is represented; note that for loop 1 (through interception), a coupling cannot be distinguished from storm-scale precipitation persistence. Step B of the feedback remains a single component as the three evaporation components combine and only the total heat fluxes and their partitioning matter to precipitation formation.

Title Page

Abstract

Introduction

Conclusions

References

Tables

Figures

◀

▶

◀

▶

Back

Close

Full Screen / Esc

Printer-friendly Version

Interactive Discussion



Land surface controls on afternoon precipitation

B. P. Guillod et al.

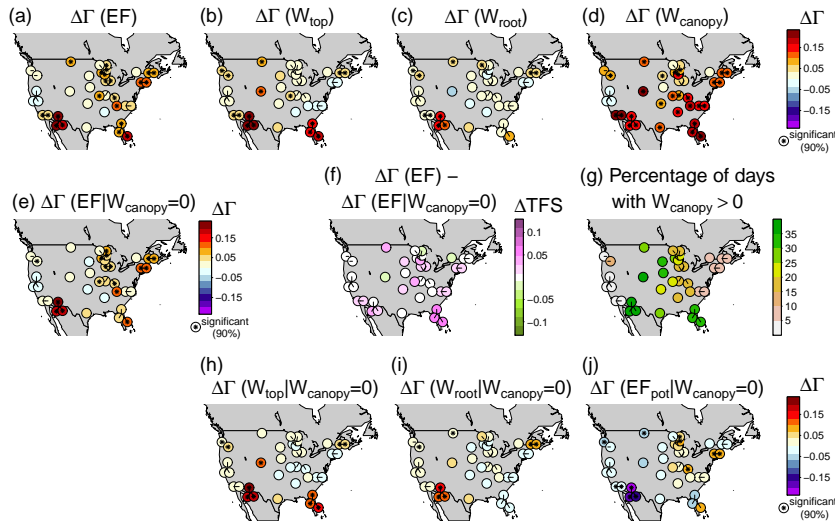


Fig. 10. Identification of the drivers of the EF-precipitation relationship in NARR. Top row: difference in the probability of afternoon rainfall ($\Delta\Gamma(X)$) on days with high vs. low X where X is a variable (before-noon value). From left to right, X is **(a)** EF and **(b–d)** the three water storage terms that control EF: **(b)** surface soil moisture (W_{top} , controls bare soil evaporation), **(c)** root zone soil moisture (W_{root} , controls plant transpiration) and **(d)** vegetation (canopy) interception storage (W_{canopy} , controls interception evaporation). Middle row: **(e)** $\Delta\Gamma(\text{EF})$ computation restricted to days without canopy storage, **(f)** difference between $\Delta\Gamma(\text{EF})$ computed with all days and with days without vegetation interception storage, and **(g)** percentage of days with interception storage. Bottom row: $\Delta\Gamma(X)$ restricted to days without interception storage where X is **(h)** surface soil moisture, **(i)** root zone soil moisture and **(j)** potential EF (EF_{pot}), defined as the EF value that corresponds to potential evaporation, i.e. with $\lambda E = \lambda E_{\text{pot}}$. EF_{pot} accounts for environmental forcings on EF such as entrainment at the boundary layer top. High (low) X refer to values higher (lower) than the 60th (40th) percentile of X , i.e. $\Delta\Gamma(X) = \Gamma(r|X > X_{\text{Q60}}) - \Gamma(r|X \leq X_{\text{Q40}})$. Values significantly different from 0 at the 90 % level are indicated by a black star.

Land surface controls on afternoon precipitation

B. P. Guillod et al.

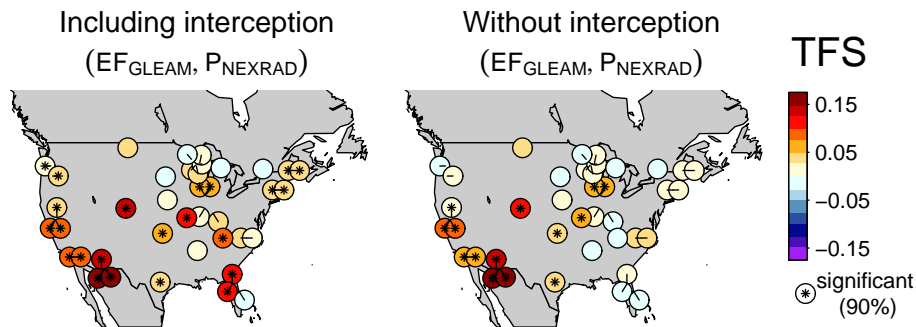


Fig. 11. Influence of interception evaporation on TFS* in the GLEAM-NEXRAD combination. Left: interception is included in the EF computation and EF is then capped to 1. Right: interception not included in the EF computation. Values significantly different from 0 at the 90 % level are indicated by a black star.

Title Page

Abstract

Introduction

Conclusions

References

Tables

Figures

◀

▶

◀

▶

Back

Close

Full Screen / Esc

Printer-friendly Version

Interactive Discussion



Land surface controls on afternoon precipitation

B. P. Guillod et al.

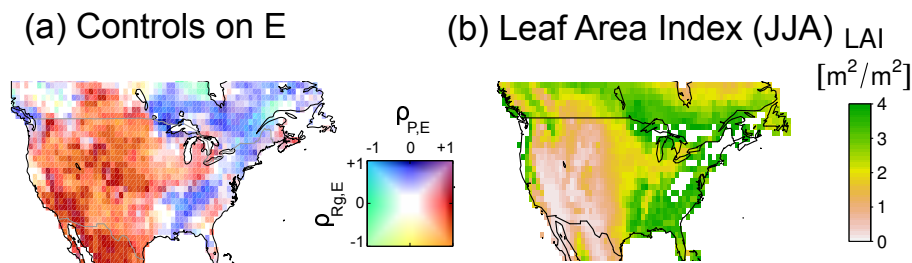


Fig. 12. (a) Land evaporation regime (blue for wet regime, red for transitional regime): multi-model analysis of controls on yearly land evaporation from Teuling et al. (2009). Correlation between yearly evaporation and global radiation ($\rho_{R_g,E}$), respectively precipitation ($\rho_{P,E}$), for the period 1986–1995. Each color corresponds to a unique combination of $\rho_{R_g,E}$ and $\rho_{P,E}$. **(b)** Mean summer (JJA) Leaf Area Index [m^2m^{-2}] over the period 1995–2007, derived with data from Stöckli et al. (2011).

[Title Page](#)
[Abstract](#)
[Introduction](#)
[Conclusions](#)
[References](#)
[Tables](#)
[Figures](#)
[◀](#)
[▶](#)
[◀](#)
[▶](#)
[Back](#)
[Close](#)
[Full Screen / Esc](#)
[Printer-friendly Version](#)
[Interactive Discussion](#)
